NATIONAL ADVISORY COMMITTEE FOR AERONAUTICS

TECHNICAL NOTE 4140

TURBULENT SHEARING STRESS IN THE BOUNDARY LAYER OF YAWED FLAT PLATES

By Harry Ashkenas

Cornell University

NACA
Washington
April 1958

1G

NATIONAL ADVISORY COMMITTEE FOR AERONAUTI(

TECHNICAL NOTE 4140

TURBULENT SHEARING STRESS IN THE BOUNDARY LAYER OF YAWED FLAT PLATES

By Harry Ashkenas

SUMMARY

Hot-wire anemometer measurements of the turbulent shearing stress in a turbulent boundary layer on a yawed flat plate are presented. Two plates with angles of yaw of 0° and 45° were studied. Measurements of the intensity of turbulence were made simultaneously with the shear measurements, using a technique developed by the author. The experimental procedure is reviewed briefly and an attempt is made to evaluate the precision of the results.

The measured velocity profiles are used to calculate the shear distribution and the result is compared with the result of experimental shear measurements.

The unyawed-flat-plate data agree well with calculated results, whereas the 45° data are apparently not amenable to calculation. Some speculative remarks are included in an attempt to explain the discrepancy.

INTRODUCTION

The problem of the turbulent boundary layer has engaged the attention of aerodynamicists for many years. The mathematical difficulties entailed in a theoretical analysis of the problem have inevitably led to a strong dependence on experimental studies. In order to obtain any insight into the turbulent boundary layer, it is necessary to consider as simple an experimental setup as possible. That is, problems of the mechanism of transition and of the behavior of a two-dimensional turbulent boundary layer without pressure gradient and similar fundamental problems have had to be attacked; though some of these problems have not been solved, at least some light has been thrown on the subject so that more complex phenomena can be studied. It is not too surprising, therefore, to find little in the literature regarding three-dimensional turbulent boundary layers, when the two-dimensional turbulent-boundary-layer problem can scarcely be considered near solution.

During the past decade, however, some interest has been shown in the problem of the turbulent boundary layer on a yawed cylinder, which is probably the simplest three-dimensional case that might be considered. The impetus to this interest in the yawed turbulent boundary layer was given primarily by the work of Prandtl (ref. 1), Jones (ref. 2), and Sears (ref. 3) who showed that for the laminar boundary layer on a yawed cylinder, the boundary-layer equations in the chordwise direction are independent of the flow along the span; that is, the flow past a yawed cylinder may be expressed in terms of the flow at right angles to the same cylinder. "Simple sweep theory" or "independence principle" are two of the terms used to describe this property.

Such a simple principle for yawed flows is quite attractive from the point of view of the turbulent boundary layer. Unfortunately, the applicability of the independence principle to the turbulent case cannot be settled analytically, since the shear law is not simple nor accurately known for a turbulent boundary layer. Recourse had to be made to experiment.

Kuethe, McKee, and Curry (ref. 4) conducted experiments using a yawed finite wing. Measurement and analysis of the velocity profiles indicated that the chordwise velocity profiles agreed with the results of a similar analysis for unswept wings. When they attempted to calculate the chordwise velocity profiles from the unswept-wing data, however, the experimental and calculated velocity profiles did not agree.

Altman and Hayter (ref. 5) present boundary-layer profiles and flow directions for the case of a two-dimensional wing at 0° and 45° angles of yaw, with transition artificially fixed near the leading edge. Although Altman and Hayter concluded that the independence principle was valid, Turcotte (ref. 6) has shown that these data can be better represented by considering that the yaw has no effect on the boundary-layer growth. Turcotte has included in his analysis a second-order approximation to the boundary-layer equations, for the case of turbulent flow. This approximation includes fluctuating velocity terms which are usually neglected. Turcotte's analysis of the problem included the effect of pressure gradient; he found that for appreciable pressure gradients the growth of the turbulent boundary layer was most influenced by the pressure term in the momentum equations. Thus, almost any reasonable estimate of the wall shear would give a result in fair agreement with a measured growth law. Young and Booth (ref. 7), without theoretical justification, applied the independence principle to the turbulent boundary layer and compared their calculations with measurements of the drag of a flat plate equipped with a leading-edge trip wire at several angles of yaw. They also measured the boundary-layer profile at one station on the plate, again for several angles of yaw. Their experimental results tended to confirm the validity of the independence principle for the turbulent boundary layer. Unfortunately, the experimental setup and

techniques used were not described in sufficient detail to enable an estimate to be made of the reliability of this important result.

Accordingly, Ashkenas and Riddell undertook the experimental program described in reference 8. Measurements were made on three yawed flat plates, with angles of yaw of 0°, 30°, and 45°. A sandpaper boundary-layer trip was affixed to the leading edge of each plate, and measurements were made of the boundary-layer growth as well as of the flow direction in the boundary layer. These experiments indicated that the growth of the turbulent boundary layer on a yawed flat plate could not be computed using the independence principle. In fact, the effect of yaw was in the opposite direction to that predicted by the assumption of the independence principle.

The present investigation, then, has had as its primary purpose, the exploration of the results of reference 8. To this end, detailed measurements of the turbulent shearing-stress distributions have been made in the boundary layers of the 0° and 45° plates. The instrument chosen for the bulk of the experiments was, of necessity, the hot-wire anemometer. Prior to embarking on the present investigation, an intensive program of development of a method for obtaining reliable shear readings from an X-type hot-wire anemometer was undertaken. The results of this program are presented in reference 9, in which a technique of calibration and calculation is described that appears to give reliable results.

The investigation was conducted at Cornell University under the sponsorship and with the financial assistance of the National Advisory Committee for Aeronautics. The author wishes to express his appreciation to Profs. W. R. Sears, Y. H. Kuo, and N. Rott of the staff of the Graduate School of Aeronautical Engineering for their interest and many valuable discussions. Messrs. J. Cassidy, M. Fiebig, R. Hunt, and K. Toba assisted in carrying out the experimental program and their contributions are gratefully acknowledged.

SYMBOLS

C intercept, law of the wall, 5.1

e instantaneous hot-wire voltage

$H = \delta^*/\delta$

i current

q_1	free-stream dynamic pressure, $\frac{1}{2}\rho U_1^2$
R	hot-wire resistance in heated condition
R_a	hot-wire resistance at ambient temperature
U,V,W	mean velocity components in ξ,η,z coordinates
U_1	free-stream velocity
U_τ	friction velocity, $\sqrt{\tau_w/\rho}$
u,v,w	instantaneous velocity components in ξ,η,z coordinates
x	distance from leading edge, law of the wall
δ	boundary-layer thickness, defined by $\left(\delta^* U_1/U_\tau\right)\kappa/(1+\pi)$
δ^*	boundary-layer displacement thickness, $\int_0^\delta \left(1 - U/U_1\right)dz$
ϑ	boundary-layer momentum thickness, $\int_0^\delta U/U_1\left(1 - U/U_1\right)dz$
κ	slope of law of the wall, 0.4
Λ	angle of yaw of flat plate
μ	absolute viscosity
ν	kinematic viscosity
ξ,η,z	coordinate system defined in figure 13
ξ_o	virtual origin of turbulent boundary layer
π	wake profile parameter, law of the wake
ρ	air density
τ	total shearing stress, $\mu\frac{\partial U}{\partial z} + \rho\overline{uw}$
τ_w	shearing stress at wall

φ angle of yaw of hot wire

ω wake profile function

A prime denotes root-mean-square value. A bar denotes a mean value.

EXPERIMENTAL EQUIPMENT AND METHODS

The unyawed plate and the 45° plate of reference 8 were used for these experiments. A 1-inch strip of sandpaper $\frac{1}{4}$ inch from the leading edge was used as a boundary-layer trip, as in reference 8. The plates were installed near the beginning of the 6- × 3- × 30-foot test section of the low-turbulence, low-speed wind tunnel described in reference 8. In all respects, the test conditions of reference 8 were duplicated as closely as possible; part of the side wall of the tunnel which had been removed for the earlier experiments on the unyawed plate was replaced for the tests on the 45° plate. This wall was not removed when the new measurements were made on the unyawed plate. Aside from this, the experimental environment was the same as that of reference 8.

All measurements reported herein were made at a constant value of the Reynolds number per foot, for example, $U_1/\nu = 250{,}000$. The daily variation of atmospheric pressure and wind-tunnel temperature was compensated for by variations in the tunnel velocity. This compensation is by no means trivial for this particular wind tunnel; the tunnel air temperature varies from a wintertime low of 20° F to a summertime high of 110° F.

The pressure distribution on the plates was determined from static-pressure orifices in the plates themselves and also from a static-pressure probe taped to the plate at various positions. Static pressures were read on an alcohol manometer equipped with a microscope and reticle having a least count of 0.001 inch.

Mean velocity profiles were measured with a flattened hypodermic-tubing total-head probe. Traversing through the boundary layer was accomplished by means of the mechanism shown in figure 1 (Mr. R. Hunt designed the traversing mechanism). The mechanism features a micrometer adjustment for translating the probe through the boundary layer, as well as a micrometric angular positioning device (for angular rotation in the horizontal plane) together with a simple protractor for vertical rotation. The traversing head is pictured in working position in figure 1(a). The actuating mechanism, mounted outside the wind tunnel, is shown in figure 1(b). The method of determining the zero position of the

total-head tube is described in reference 8. The remarks in reference 8 concerning the various manometers used apply here as well.

The zero setting of the traversing mechanism with an X-meter in place was accomplished by means of a simple scale measurement from the wall to the hot wire. Using a steel scale with 1/50-inch graduations, the position of the center of the X-meter could be determined to within ±0.005 inch. Since the aerodynamic center of the X-meter was unknown, there was no point in attempting to locate the probe with any more accuracy. This procedure gives rise to a possible position error as the wall is approached and will be discussed later.

All boundary-layer traverses were made in two phases. A series of points was measured through the boundary layer and then a second series of points between the first set was measured to complete the traverse.

A complete and detailed description of the hot-wire anemometry equipment and the mode of operation has been given in reference 9. For easier reference, a brief résumé of this report will be included here. The hot-wire probe itself is of conventional aspect. Four-hole ceramic tubing, protected by a brass tube, carries copper wire soldered to no. 10 sewing needles which in turn support the jeweler's broaches to which a 0.0001-inch wire of 10 percent rhodium and 90 percent platinum is soft soldered. Flexible-wire leads from the probe are connected at the plate surface to the Wheatstone bridge cables. This connection is visible in figure 1(a). The length of the X-meter wires varied between 0.050 and 0.010 inch. No effect of length was noted in the results; hence, all the measurements reported here are uncorrected for the finite length of the wire.

The electronic equipment used was again of conventional design and requires no lengthy description. It is only necessary to say that the complete setup entails the use of a square-wave generator for determining the time constant of the wire, a Wheatstone bridge and associated switching devices, a single resistance-capacitance compensated amplifier with differential input and single-ended output, a 10-kilocycle filter for restricting the band width of the amplifier, and a balanced triode metering circuit with a vacuum thermocouple as detector.

The principal measurements to be made in the operation and calibration of the hot wire include direct-current resistances, currents, and voltages and alternating-current voltages. Resistance measurements are made by means of the Wheatstone bridge; direct currents and voltages, by means of a Leeds and Northrup K-2 potentiometer; alternating-current voltages are determined by matching the hot-wire output on the thermocouple microammeter with a known alternating-current voltage supplied by a sine-wave-generator—General Radio Micro-volter combination.

X-Meter Technique

The technique of calibration and of data reduction for the X-meter was that reported in reference 9. Briefly, the method consists of considering the voltage fluctuation of a yawed hot wire as being made up of two linear components, that is, for a two-wire meter, as shown in the following equations:

$$\left.\begin{aligned} e_1 &= u\frac{\partial e_1}{\partial u} + w\frac{\partial e_1}{\partial w} \\ e_2 &= u\frac{\partial e_2}{\partial u} + w\frac{\partial e_2}{\partial w} \end{aligned}\right\} \tag{1}$$

To determine the shear stress, $\overline{e_1^2}$, $\overline{e_2^2}$, and $\overline{(e_1 - e_2)^2}$ are measured, giving

$$\left.\begin{aligned} \overline{e_1^2} &= \overline{u^2}\left(\frac{\partial e_1}{\partial u}\right)^2 + 2\overline{uw}\left(\frac{\partial e_1}{\partial u}\frac{\partial e_1}{\partial w}\right) + \overline{w^2}\left(\frac{\partial e_1}{\partial w}\right)^2 \\ \overline{e_2^2} &= \overline{u^2}\left(\frac{\partial e_2}{\partial u}\right)^2 + 2\overline{uw}\left(\frac{\partial e_2}{\partial u}\frac{\partial e_2}{\partial w}\right) + \overline{w^2}\left(\frac{\partial e_2}{\partial w}\right)^2 \\ \overline{(e_1 - e_2)^2} &= \overline{u^2}\left(\frac{\partial e_1}{\partial u} - \frac{\partial e_2}{\partial u}\right)^2 + 2\overline{uw}\left(\frac{\partial e_1}{\partial u} - \frac{\partial e_2}{\partial u}\right)\left(\frac{\partial e_1}{\partial w} - \frac{\partial e_2}{\partial w}\right) + \overline{w^2}\left(\frac{\partial e_1}{\partial w} - \frac{\partial e_2}{\partial w}\right)^2 \end{aligned}\right\} \tag{2}$$

If the wire voltages and the static derivatives are known, the foregoing set of equations may be solved for the three unknowns, $\overline{u^2}$, $\overline{uw}$, and $\overline{w^2}$, giving the turbulent shearing stress simultaneously with the intensity measurement. The static derivatives are determined for each wire (and, incidentally, each run) by calibration.[1] The calibration procedure is divided into three parts. These are:

---

[1]The use of separate u and w calibrations for an X-meter was first suggested to the author by Professor S. Corrsin of the Johns Hopkins University.

(1) Direct-current wire voltage against angle of yaw φ for fixed air speed. A seven-point traverse is made in equal increments about a zero position. The method of Ehrich (ref. 10) is used to fit a least-square parabola to the data and the derivative $\frac{\partial e}{\partial \varphi} \approx \frac{\partial e}{\partial\left(\frac{w}{U}\right)}$ is determined.

(2) Direct-current wire resistance against airspeed, for quasi-constant current operation; that is, Ruetenik's "hands off" method (ref. 11) is used to approximate the dynamic characteristic of the wire. A King's law plot $R/(R - R_a)$ against $\sqrt{U}$ of these data gives $\frac{\partial R}{\partial U}$.

(3) Direct wire current against airspeed. A straight-line approximation to these data is made, giving $\frac{\partial i}{\partial U}$.

Parts (2) and (3) taken together give

$$\frac{\partial e}{\partial U} = i \frac{\partial R}{\partial U} + R \frac{\partial i}{\partial U}$$

In practice, all wires were calibrated both before and after each run. In very few cases did the wire calibrations change appreciably, although runs of up to 6 hours duration were frequently made. It is believed that this consistency of calibration is primarily due to the lack of dust in the airstream, which in turn is a consequence of the screen installation at the contraction entrance. A 50-mesh stainless-steel screen serves as an efficient dust collector.

The author believes that the method of reference 9 has several advantages over other methods of shear measurement. Chief among these is the fact that no assumption is made regarding the cooling law of the hot wire. No hot-wire matching technique is necessary. The orientation of the X with respect to the mean flow need not be known, since the meter is calibrated and the measurements are made with the wire in the same position. The shear is measured simultaneously with the turbulence intensities.

The primary disadvantages of the method lie in the length of calibration time and in the fact that three simultaneous equations must be solved to reduce the data. The use of high-speed digital computing equipment greatly lessens the labor involved in this latter disadvantage. This was the case for the data that will be presented later. Equations (2), for each run, were solved by means of the card programmed computer of the Cornell Computing Center.

The accuracy of the method is illustrated by the results of reference 9, where the measured turbulent shearing stress in a circular pipe is compared to the value computed from the pressure drop along the pipe. The experimental accuracy, close to the wall (the most critical region) was of the order of ±10 percent. Away from the wall, the accuracy improves to about ±5. Some of the results presented in this report show single-point deviations greater than those mentioned; these appear to be the result of undetected errors in the measurements and/or the data reduction and should be considered accordingly. In order to achieve these results great precision is required in the measurement of the calibration constants. An examination of the orders of magnitude involved in equations (2) reveals that in each of the three equations the shear term is the smallest, so that, effectively, the shear measurements are small differences between two large numbers. As an example of the precision required, it was found that a 5-percent error in the $\frac{\partial e}{\partial U}$ term results in a 10-percent error in the measured shear. Thus, in the experiments, all runs in which the measured slopes of the curves of $\sqrt{U}$ against $R/(R - R_a)$ changed by more than 3 percent from beginning to end of the calibration were discarded. Similar considerations apply to the calibration constant $\frac{\partial e}{\partial w}$. Considerably more data were taken, therefore, than are presented here. Only those data which showed consistency in calibration and result were retained.

EXPERIMENTAL RESULTS AND DISCUSSION

Pressure Distributions

The pressure distributions along the plates in the regions where profile measurements were taken are shown in figures 2 and 3. Figure 2 gives the distribution for the 0° plate and figure 3 that for the 45° plate. It will be noted that the pressure does not vary by more than ±1 percent of q_1, the free-stream total head, over almost the entire plate. These measurements were repeated during the course of the experiments in order to insure that the flow conditions had not changed.

Hot-Wire Anemometer Results

In figures 4 to 9 the results of the measurements are presented. The unyawed plate was studied at only three stations, 24, 36, and 47 inches from the leading edge (the plate chord is 48 inches). In figure 4, u'/U and U/U_1 are shown for each of these three stations.

The term u'/U is derived from the X-meter data; the term U/U_1 is derived from Pitot tube measurements. Figure 5 depicts the w'/U distributions as calculated from the X-meter data, while figure 6 presents the shearing-stress results.

For the case of the 45°-yawed plate, six stations were completely surveyed. These were at 8, 24, 36, 44, 54, and 66 inches from the leading edge (measured in a streamwise direction). Again the chord of the plate is 4 feet, but the streamwise length of the plate is approximately 71 inches. In a similar fashion to that for the 0° plate, figures 7, 8, and 9 show $\frac{u'}{U}$ and $\frac{U}{U_1}$, $\frac{w'}{U}$, and $\frac{\overline{uw}}{U_1^2}$, respectively, for the plate with leading edge yawed 45°.

In each of the figures, the results of at least two runs are presented. For the 45° plate each run represents data taken with a different hot wire, generally at a different temperature (the heating currents used ranged between 20 and 25 milliamperes) and at a different orientation.

The data for the unyawed plate were all taken with the same hot wire (this represents about 40 hours of tunnel running time), but again two runs were made at each station, to test the reproducibility of the result.

Two methods were used to calculate the value of the total shear at the wall. The rate of momentum-thickness growth, was measured from the logarithmic plots of figures 10 and 11 and the wall shear was computed from the relation

$$\frac{\partial \vartheta}{\partial(\xi_o + \xi)} = \frac{\tau_w}{\rho U_1^2}$$

The wall shear was also determined by fitting the mean velocity profile to the law of the wall of reference 12 (see following section). The values determined by these two methods are shown on figures 6 and 9. The symbol $\diamond$ refers to the $\partial\vartheta/\partial(\xi_o + \xi)$ calculation and the symbol *, to the law of the wall.

Coles' Treatment of the Turbulent Boundary Layer

In order to discuss the results of the shearing-stress measurements it will be instructive to consider first the mean velocity profiles in the light of the recent work of Coles (refs. 12 and 13).

In reference 12, Coles, following Prandtl, presents the law of the wall for the turbulent boundary layer as a universal function for the flow past a smooth surface. By means of an exhaustive analysis of the mean velocity measurements of many investigators, he has tentatively arrived at the form

$$\frac{U}{U_\tau} = \frac{1}{\kappa} \log_e \frac{zU_\tau}{\nu} + C$$

as a universal velocity profile close to the wall where U_τ is defined as the friction velocity and is equal to $\sqrt{\tau_w/\rho}$. For values of zU_τ/ν less than 50 the viscous shear predominates and the assumption of a linear velocity profile in this region implies that $U/U_\tau = zU_\tau/\nu$. In reference 12, taking $\kappa = 0.4$ and $C = 5.1$, Coles presents a convenient table of the law of the wall and related functions. Given the law of the wall, it is then possible to determine the wall shearing stress merely by fitting a measured velocity profile to the tabulated data of reference 12. In order to be able to specify the complete velocity profile of the turbulent boundary layer, Coles, in reference 13, proposes an additional function to be added to the law of the wall. By considering the departure from the law of the wall of the mean velocity profiles of several investigations in widely differing flow environments, Coles arrives at a universal "wake function" of z/δ, so that the complete boundary-layer profile may be specified by the equation

$$\frac{U}{U_\tau} = \frac{1}{\kappa} \log_e \frac{zU_\tau}{\nu} + C + \frac{\pi(x)}{\kappa} \omega\left(\frac{z}{\delta}\right)$$

where $\omega(z/\delta)$ represents the wake profile, a tabulation of which, together with various related functions, is given in reference 13. The symbol π is referred to as a profile parameter and represents the amount of the wake function which must be added to the law of the wall to obtain a given velocity profile. Thus, if the tabulated functions of references 12 and 13 are truly universal, it should be possible, by a suitable choice of the parameters $\frac{U_1}{U_\tau}$ and π, to fit almost any given two-dimensional, incompressible, turbulent-boundary-layer velocity profile. Once the values of $\frac{U_1}{U_\tau}$ and π have been established, a completely analytic form of the mean velocity distribution is available for insertion into the boundary-layer equations of motion for calculation of the shearing-stress distribution.

In figures 11 and 12, the mean velocity profiles measured during the course of the present investigation are depicted in semilogarithmic plots, using the coordinates $\frac{U}{U_\tau}$ against $\log \frac{zU_\tau}{\nu}$. Figure 12(a) gives the results for the case of $\Lambda = 0^\circ$ and figure 12(b), the results for $\Lambda = 45^\circ$. The values of $\frac{U_1}{U_\tau}$ which were used in plotting these data were determined, as described above, by fitting the data to the tabulation of the law of the wall in reference 12. The law of the wall is shown by the dashed line in figures 12(a) and 12(b). It is seen that the fit for both the yawed and unyawed plates is quite good in the region of validity of the law of the wall. The departure from the universal curve in the viscous region close to the wall is possibly due to the influence of the turbulence level on the Pitot tube measurements (the measurements are uncorrected for this effect) or perhaps is due to a position error in the measurement of the distance from the wall. No correction was made for the displacement of the effective center of the probe in the steep velocity gradient near the wall. The points which depart from the curve are all within 0.012 inch from the wall and are highly susceptible to position error. It should be noted, however, that this departure from the universal curve is in opposite directions for the yawed and unyawed plates.

In addition to the law of the wall, the data shown in figures 11 and 12 are also fitted to Coles' law of the wake, using the tabulated values of the wake function given in reference 13. The values of π and $\frac{U_1}{U_\tau}$ which were used in this fitting process are given in table I, together with other pertinent boundary-layer parameters. The wake profile is shown by the solid curves of figures 12(a) and 12(b).

Although Coles makes no claim that the tabulated functions of references 12 and 13 may be fitted to a yawed boundary-layer profile, it is seen from figures 12(a) and 12(b) that a remarkably good fit has been obtained for both the yawed and unyawed data.

Using the data of table I, the analytic representation of the mean velocity profile has been used, together with the boundary-layer equations of motion, to compute the shearing-stress distribution as outlined by Coles in reference 13. These calculated profiles are shown as the solid curves of figures 6(b), 9(b), 9(d), and 9(f).

In figure 6(b), the agreement between experimental and calculated values of the shear stress is quite striking. The figure presents an effective argument for Coles' approach to the problem of calculating the turbulent shearing stress on an unyawed flat plate.

The measured shear profiles for the yawed plate present a different picture however. An examination of all the components of figure 9 reveals a peculiar behavior of the shear-stress profiles close to the wall. In particular, the data at the 36-, 44-, and 54-inch stations exhibit a noticeable maximum in the shear at a point about 0.75δ^* away from the wall. These maxima can be clearly seen in the data of all the runs that are presented herein; the same qualitative behavior existed in runs which were discarded for poor calibrations. In figure 9(d) at $\xi = 44$ inches, the calculated curve of the turbulent shear stress is compared with the experimental points. Although a maximum does exist in the calculated curve due to the subtraction of the viscous shear from the total shear, it is seen that the agreement between experiment and calculation is not nearly so good as it is in the case of the unyawed plate. The same is true for the comparisons shown in figures 9(b) and 9(f) at $\xi = 24$ and 66 inches, respectively. Calculation and experiment, while not in strong disagreement, are sufficiently different so that one seeks the reason for the disparity.

Remarks on the Shear Distribution Calculation

In reference 13, Coles has considered the problem of the boundary layer on a yawed wing (using the data of ref. 4). In the case that he has treated, however, considerable flow deviation from the mean stream was measured, making it necessary to treat the wake and wall components of the boundary layer as vector components instead of as scalars. As shown in reference 8, however, the present case is one in which the maximum flow deviation from the free-stream direction was of the order of 3° and is thus a negligible factor. A further argument in favor of a scalar addition of the wall and wake components for the present data is given by the agreement noted in figure 12(b).

A possibility which must be considered is that the equation of motion used by Coles in calculating the shear stress neglects certain terms that may be of nonnegligible magnitude. This proposition has been investigated by Turcotte, reference 6, who made the boundary-layer approximation to the equations of motion including second-order terms. In the coordinate system shown in figure 13, Turcotte's equation of motion for zero pressure gradient is

$$U\frac{\partial U}{\partial \xi} + W\frac{\partial U}{\partial \xi} = \frac{1}{\rho}\left(\mu\frac{\partial^2 U}{\partial z^2} - \rho\frac{\partial \overline{uw}}{\partial z} - \rho\frac{\partial \overline{u^2}}{\partial \xi} + \rho\frac{\partial \overline{uv}}{\partial \xi}\right)$$

This equation is the same as the usual boundary-layer form, except for the two additional terms on the right-hand side. During the course

of the present investigation measurements of $\overline{uv}$ were made in an effort to evaluate the magnitude of the term $\frac{\partial \overline{uv}}{\partial \xi}$.

These measurements are not presented here in detail, since there is some question as to their validity. The results indicated that $\overline{uv}$ was quite small, of the order of $\frac{1}{4}\overline{uw}$. The loss of accuracy in the measurement due to the small $\overline{uv}$ signal was enough to make the experimental scatter excessive. Nevertheless, in order to give some idea of the order of magnitude of the term, figure 14 shows the results of these preliminary and somewhat questionable measurements. In figure 14, the value of $\overline{uv}/U_1^2$ at $z = 0.172$ inch (which is equal to δ^* for the data 44 inches from the leading edge) in the 45° yawed flat plate is shown as a function of ξ, the distance from the leading edge. The values of $\partial\left(\overline{uv}/U_1^2\right)/\partial\xi$ derived from the straight line drawn through these points is -6.3×10^{-6} per inch. This may be compared with the value of $\partial\left(\overline{uw}/U_1^2\right)/\partial z$ at the same distance from the wall evaluated from the measurements at $\xi = 44$ inches. This value, also noted on figure 14, is seen to be -7.75×10^{-4} per inch. The $\overline{uv}$ term, from these data, is apparently less than 1 percent of the $\overline{uw}$ term and its contribution although in the right direction (i.e., to be subtracted from the total shear to give $\overline{uw}$) is indeed negligible.

Also shown in figure 14 is the quantity $\left(\overline{u^2}/U_1^2\right)$ as a function of ξ at $z = 0.172$ inch. This curve is, for all practical purposes, a horizontal line, indicating that $\partial\left(\frac{\overline{u^2}}{U_1^2}\right)\Big/\partial\xi$ in Turcotte's equation is also of small importance.

The question remains, then, as to the discrepancy between experiment and calculation. The difficulty of advancing any convincing remarks concerning the relationship between the experimental results and the calculations lies in the fact that, given the correct velocity profile and assuming that no important terms have been neglected in the equations of motion, the calculated result must be the correct one.

On the other hand, the question arises as to just how sensitive the calculated shear distribution is to small changes in the velocity profile. While making the calculations of the shearing-stress distribution, the author was struck by the fact that the end points of the shear curve are fixed by the values chosen for $\frac{U_1}{U_\tau}$ and δ, and the speculation arose that perhaps any reasonable form for the velocity

profile would give good results for the shear, provided the values chosen for $\frac{U_1}{U_\tau}$ and δ were correct. In order to test this hypothesis, a 1/7th-power-law velocity profile was assumed; that is,

$$\frac{U}{U_1} = \left(\frac{z}{\delta}\right)^{1/7}$$

Using this profile, the growth law of the boundary layer (see, for instance, ref. 14) is

$$\delta = 0.37\left(\frac{\nu}{U_1 \xi}\right)^{1/5} \xi$$

The equations of motion for the case of zero pressure gradient are

$$U \frac{\partial U}{\partial \xi} + W \frac{\partial U}{\partial z} = \frac{1}{\rho} \frac{\partial}{\partial z}\left(\mu \frac{\partial U}{\partial z} - \rho \overline{uw}\right)$$

$$= \frac{1}{\rho} \frac{\partial \tau}{\partial z}$$

$$\frac{\partial U}{\partial \xi} + \frac{\partial W}{\partial z} = 0$$

so that

$$\frac{1}{\rho} \int_0^z d\tau = \int_0^z \left[U \frac{\partial U}{\partial \xi} - \left(\int_0^z \frac{\partial U}{\partial \xi} \, dz \right) \frac{\partial U}{\partial z} \right] dz$$

The terms in this equation may be evaluated from the velocity profile and growth law to give

$$\frac{\tau_w - \tau}{\rho U_1^2} = (0.037) \frac{7}{9} \left(\frac{z}{\delta}\right)^{9/7} \left(\frac{\nu}{U_1 \xi}\right)^{1/5}$$

This equation was evaluated for the station 44 inches from the leading edge of the 45° yawed plate. The value of U_1/U_τ given by the law of the wall (as shown in fig. 12) was used to determine the wall shear, τ_w. Values of δ and ξ were chosen so as to force the shear curve to approach 0 at the same value of z/δ^* as does the Coles calculation. The shear curve calculated in this fashion is shown in figure 8(d) as the dashed curve. It is seen that the differences between this result and that of the Coles method are quite small. The velocity profile, using the 1/7th-power law, is compared with the experimental points and the law of the wall (law-of-the-wake profile) in figure 15. The fit is not nearly so close as that of the wall-wake profile but, as stated previously, once the end points of the shear profile have been fixed, almost any reasonable velocity profile will result in the calculation of a reasonable shear distribution.

This state of affairs has characterized the semiempirical calculation of turbulent boundary layers since the first calculations based on the mixing-length theory appeared; that is, calculations based on the mean velocity profile are relatively insensitive. A more fundamental quantity is the turbulent shearing stress, and an understanding of the basic phenomena related to it must exist before any precise conclusions can be drawn. As the situation is today, there are few reports in which reliable turbulent-shearing-stress measurements are presented. It is to be hoped that further research will result in data, which, after searching analysis, will yield a workable semiempirical theory of turbulent shear flows.

For the present, there is still the question of the behavior of the experimental shear profile close to the wall, since neither method of calculation of the shear profile predicts the behavior illustrated. It is possible that the assumptions made in writing the equation of motion were incorrect. The departures from these assumed conditions are relatively small:

(1) The flow is not everywhere parallel to the free-stream direction within the boundary layer.

(2) There is a small, but noticeable, difference in the assumed velocity profile close to the wall.

(3) Some terms in the equations of motion, which may be appreciable, have been neglected.

It may well be that the differences shown in figure 9 are due to a combination of the effects of these three points. The only other source of error which comes to mind is that of the experimental environment in which the measurements were made. That is, the measurements

may not actually have been made in a fully developed, two-dimensional, turbulent boundary layer with zero pressure gradient. The question of two-dimensionality has been discussed in some detail in reference 8. For the 45° plate, the currently measured growth of δ^* agrees with that presented in reference 8; since the two-dimensionality of the flow in the latter case was checked quite carefully (measurements of ϑ_{uv}, the crossflow momentum thickness, indicated relatively little net crossflow momentum in the test region), it is assumed that the same conditions prevailed in the present case. The pressure gradient of figure 3 would indicate no difficulty concerning that assumption. As for the fully developed nature of the boundary layer, the agreement between the measured mean velocity profiles and Coles' law-of-the-wall profile (which was derived from an examination of many fully developed turbulent velocity profiles) implies that the present profiles are also those of a fully developed turbulent boundary layer.

One further avenue of speculation is open. This is the question of the effect of yaw on a boundary-layer tripping device. Certainly it is within the realm of possibility that the yawed sandpaper produces a different effect than that of the unyawed sandpaper. It may be, for instance, that the recovery of the shear profile from the effects of a yawed trip is accomplished more slowly than it is for the unyawed sandpaper. This behavior would explain the results which were obtained. Unfortunately, no experimental data on this question are available. The only systematic study of artificial thickening devices is that of Klebanoff and Diehl (ref. 15) and that deals only with the unyawed turbulent boundary layer. The problem is an important one, which bears further investigation, for if the techniques for artificial thickening of the boundary layer cannot be used at large angles of yaw, then the present problem may be, for all practical purposes, insoluble experimentally. Without such devices, it will be difficult to produce a fully developed turbulent layer having the required two-dimensional character within the length limitation imposed by the interference from wind-tunnel walls.

CONCLUDING REMARKS

The turbulent boundary layers on two flat plates with angles of yaw of 0° and 45° have been examined extensively by means of hot-wire X-meter anemometry. The measured shearing-stress profiles have been compared with values calculated from the mean velocity profile using the results of Coles. Agreement between calculated and measured values of the shearing stress on the unyawed plate is excellent. Calculated

and measured values of the shearing stress for the plate yawed 45° reveal a small but systematic deviation which cannot be readily explained.

Cornell University,
Ithaca, N. Y., October 5, 1956.

REFERENCES

1. Prandtl, L.: On Boundary Layers in Three-Dimensional Flow. Reps. and Translations No. 64, British M.A.P. Völkenrode, May 1, 1946.

2. Jones, Robert T.: Effects of Sweep-back on Boundary Layer and Separation. NACA Rep. 884, 1947. (Supersedes NACA TN 1402.)

3. Sears, W. R.: The Boundary Layer of Yawed Cylinders. Jour. Aero. Sci., vol. 15, no. 1, Jan. 1948, pp. 49-52.

4. Kuethe, A. M., McKee, P. B., and Curry, W. H.: Measurements in the Boundary Layer of a Yawed Wing. NACA TN 1946, 1949.

5. Altman, John M., and Hayter, Nora-Lee F.: A Comparison of the Turbulent Boundary-Layer Growth on an Unswept and a Swept Wing. NACA TN 2500, 1951.

6. Turcotte, Donald Lawson: On Incompressible Turbulent Boundary Layer Theory Applied to Infinite Yawed Bodies. (Contract AF 33 (038)-21406)) Cornell Univ., Sept. 1955.

7. Young, A. D., and Booth, T. B.: The Profile Drag of Yawed Wings of Infinite Span. Rep. No. 38, The College of Aero. (Cranfield), May 1950.

8. Ashkenas, Harry, and Riddell, Frederick Raymond: Investigation of the Turbulent Boundary Layer on a Yawed Flat Plate. NACA TN 3383, 1955.

9. Ashkenas, Harry: Hot-Wire Measurements With X-Meters. Contract NAw-6295, NACA and Cornell Univ., May 1955.

10. Ehrich, Fredric F.: Differentiation of Experimental Data Using Least Squares Fitting. Jour. Aero. Sci. (Readers' Forum), vol.22, no. 2, Feb. 1955.

11. Ruetenik, J. Ray: Investigation of Equilibrium Flow in a Slightly Divergent Channel. Tech. Rep. No. I-19, (Navy Contract N-onr 248(33)) The Johns Hopkins Univ. Inst. for Cooperative Res., 1954.

12. Coles, Donald: The Law of the Wall in Turbulent Shear Flow. 50 Jahre Grenzschichtforschung, Friedr. Viewig & Sohn (Braunschweig), 1955, pp. 153-163.

13. Coles, Donald: The Law of the Wake in the Turbulent Boundary Layer. Jour. Fluid Mech., vol. 1, pt. 2, July 1956, pp. 191-226.

14. Fluid Motion Panel of the Aeronautical Research Committee and Others: Modern Developments in Fluid Dynamics. Vols. I and II, S. Goldstein, ed., The Clarendon Press (Oxford), 1938.

15. Klebanoff, P. S., and Diehl, Z. W.: Some Features of Artificially Thickened Fully Developed Turbulent Boundary Layers With Zero Pressure Gradient. NACA TN 2475, 1951.

TABLE I

SUMMARY OF BOUNDARY-LAYER PARAMETERS

[Obtained from mean velocity profiles]

Λ, deg	ξ, in.	$\xi_o + \xi$, in. (a)	δ^*, in.	ϑ, in.	$H = \delta^*/\vartheta$	δ, in. (b)	U_1/U_τ (c)	Π (d)	π (e)
0	24	33	0.112	0.078	1.44	0.734	23.11	0.410	0.322
0	36	45	.1375	.098	1.40	.856	23.98	.435	.435
0	47	56	.166	.121	1.37	1.104	24.36	.465	.406
45	8	17	.070	.049	1.43	.472	21.45	.28	.160
45	24	33	.109	.080	1.36	.775	22.75	.28	.189
45	36	45	.154	.111	1.39	1.046	24.12	.42	.39
45	44	53	.1725	.127	1.36	1.093	24.56	.438	.438
45	54	63	.205	.145	1.41	1.387	24.86	.47	.398
45	66	75	.228	.165	1.38	1.520	25.5	.53	.512

[a] $\xi_o = 9$ inches; see reference 8.

[b] $\delta = \left(\delta^* U_1/U_\tau\right)/(1 + \pi)$; see reference 13.

[c] U_1/U_τ obtained by fitting the mean velocity profile to law of the wall; see reference 12 and figures 12(a) and 12(b).

[d] Π obtained by fitting the mean velocity profile to law of the wake; see reference 13 and figures 12(a) and 12(b); $U_1 \approx 45$ ft/sec.

[e] π obtained from equation (17), reference 13 which is

$$2\pi - \log_e(1 + \pi) = \kappa \frac{U_1}{U_\tau} - \log_e \frac{\delta^* U_1}{\nu} - \kappa C + \log_e \frac{1}{\kappa}$$

L-57-4893

(a) Traversing head viewed from working side of plate.

Figure 1.- Traversing mechanism.

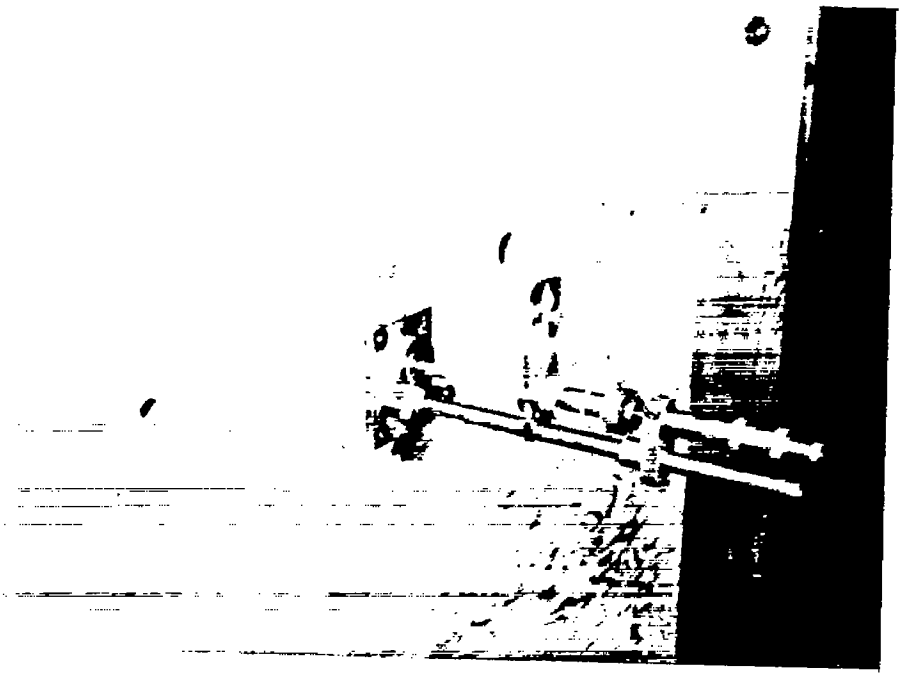

L-57-4894

(b) Traversing actuator (outside of wind tunnel).

Figure 1.- Concluded.

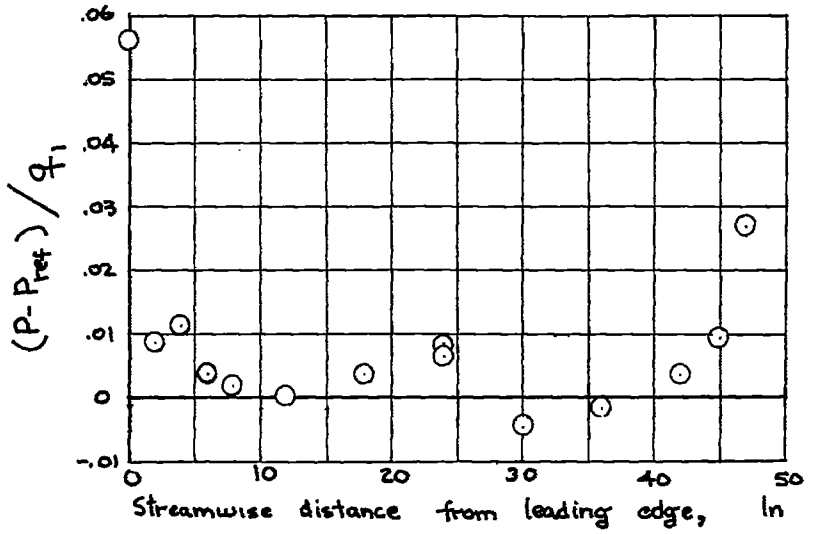

Figure 2.- Pressure distribution along center line. Re = 250,000 per foot; $\Lambda = 0°$; 1/4-inch-diameter static pressure probe 1 inch from plate surface.

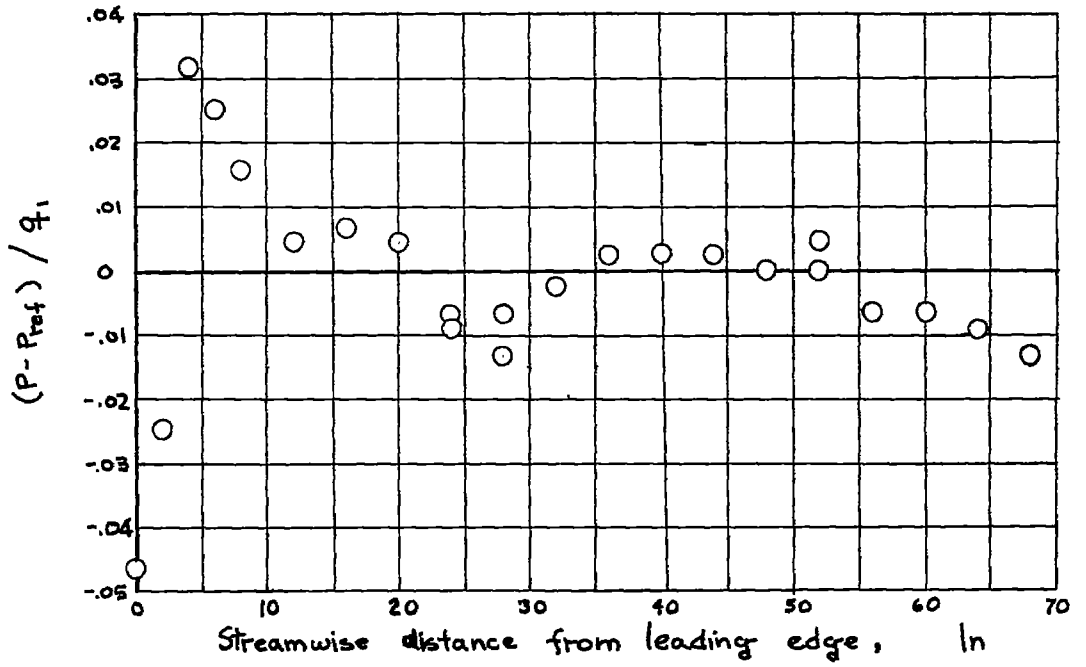

Figure 3.- Pressure distribution 10 inches above center line. Re = 250,000 per foot; $\Lambda = 45°$; 1/16-inch-diameter static pressure probe 1/4 inch from plate surface.

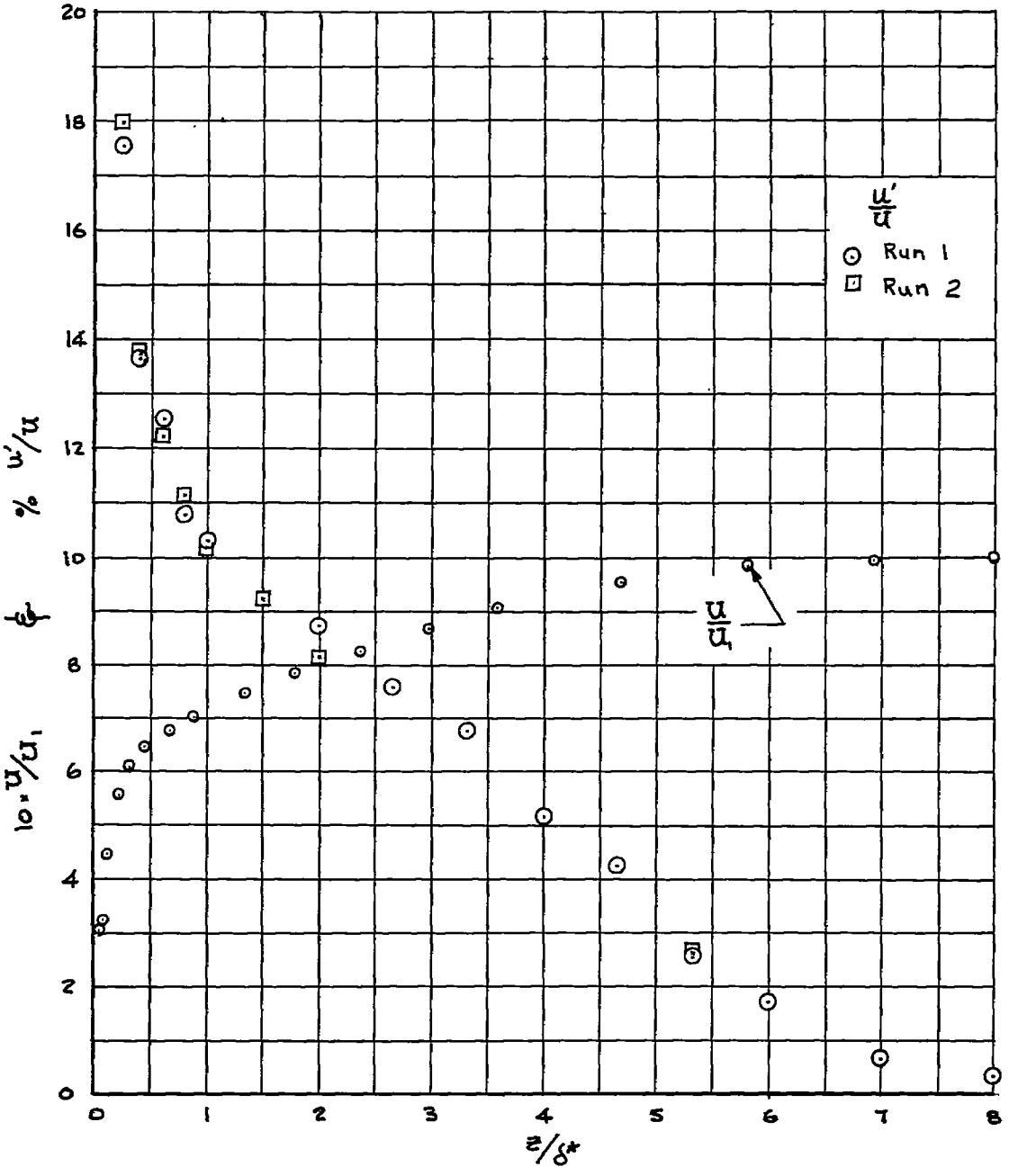

(a) $\delta^* = 0.112$ inch; $\vartheta = 0.078$ inch; measurements taken 24 inches from leading edge.

Figure 4.- Mean velocity and longitudinal turbulence intensity. $\Lambda = 0^\circ$; Re = 250,000 per foot.

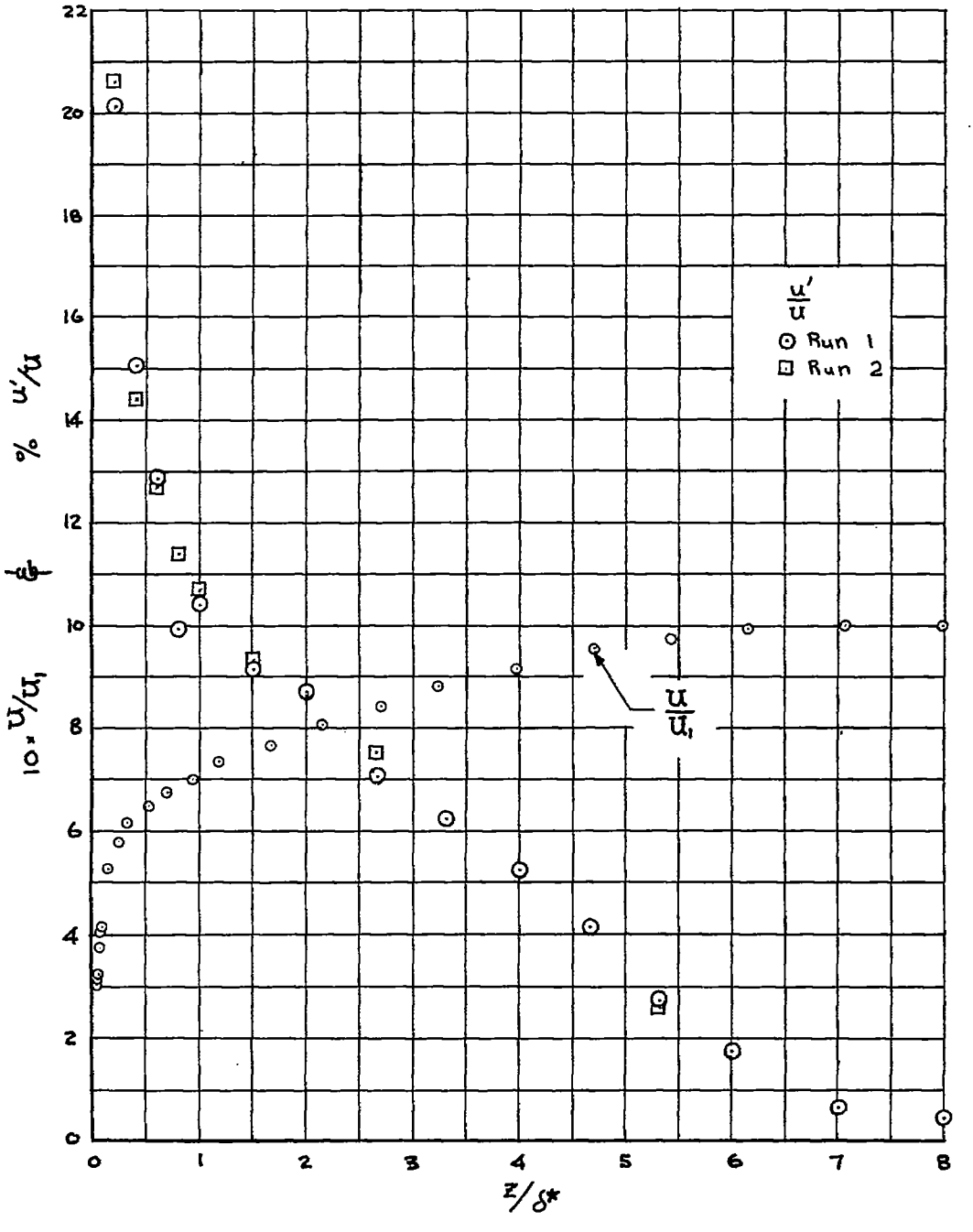

(b) $\delta^* = 0.1375$ inch; $\vartheta = 0.098$ inch; measurements taken 36 inches from leading edge.

Figure 4.- Continued.

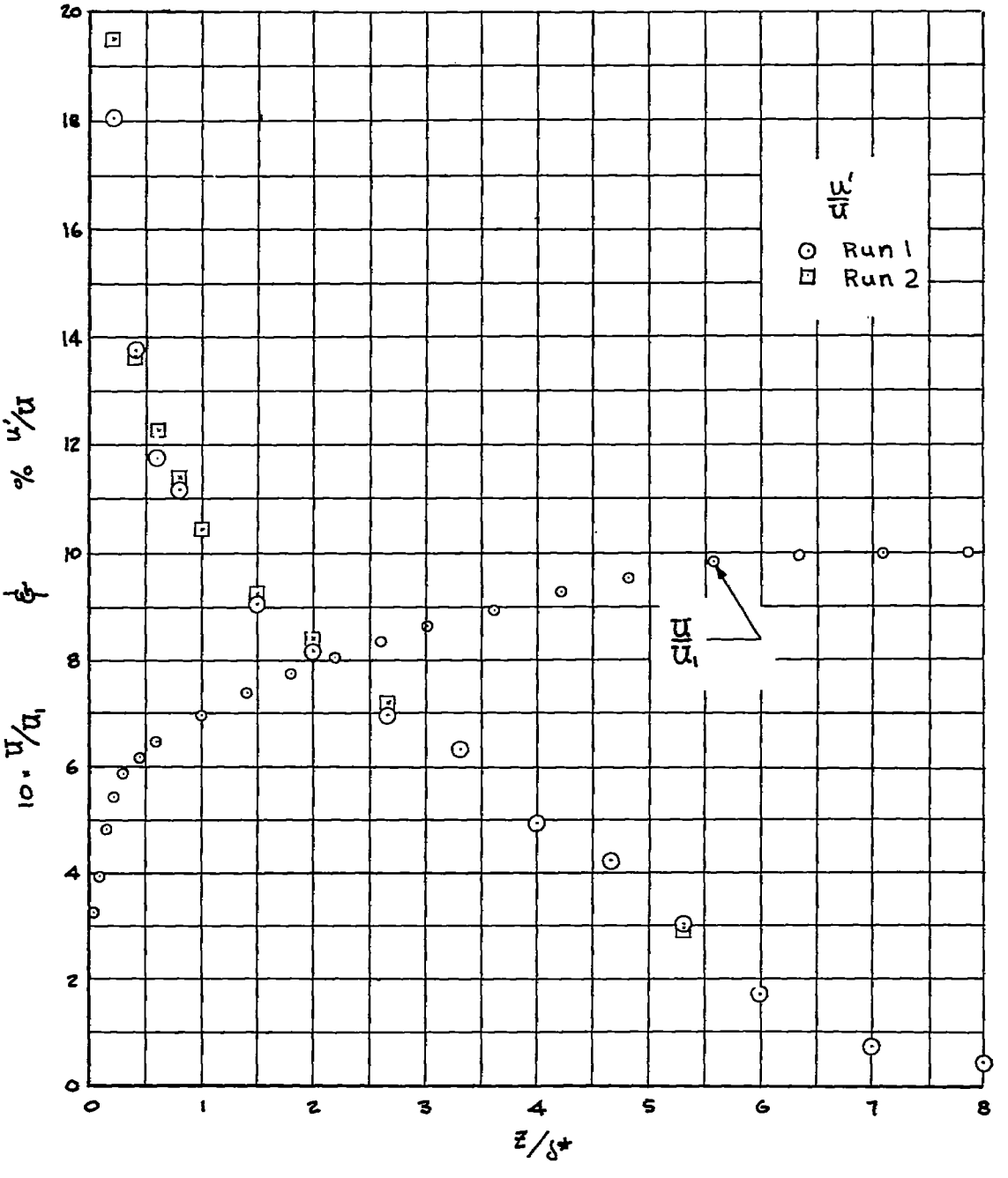

(c) $\delta^* = 0.166$ inch; $\vartheta = 0.121$ inch; measurements taken 47 inches from leading edge.

Figure 4.- Concluded.

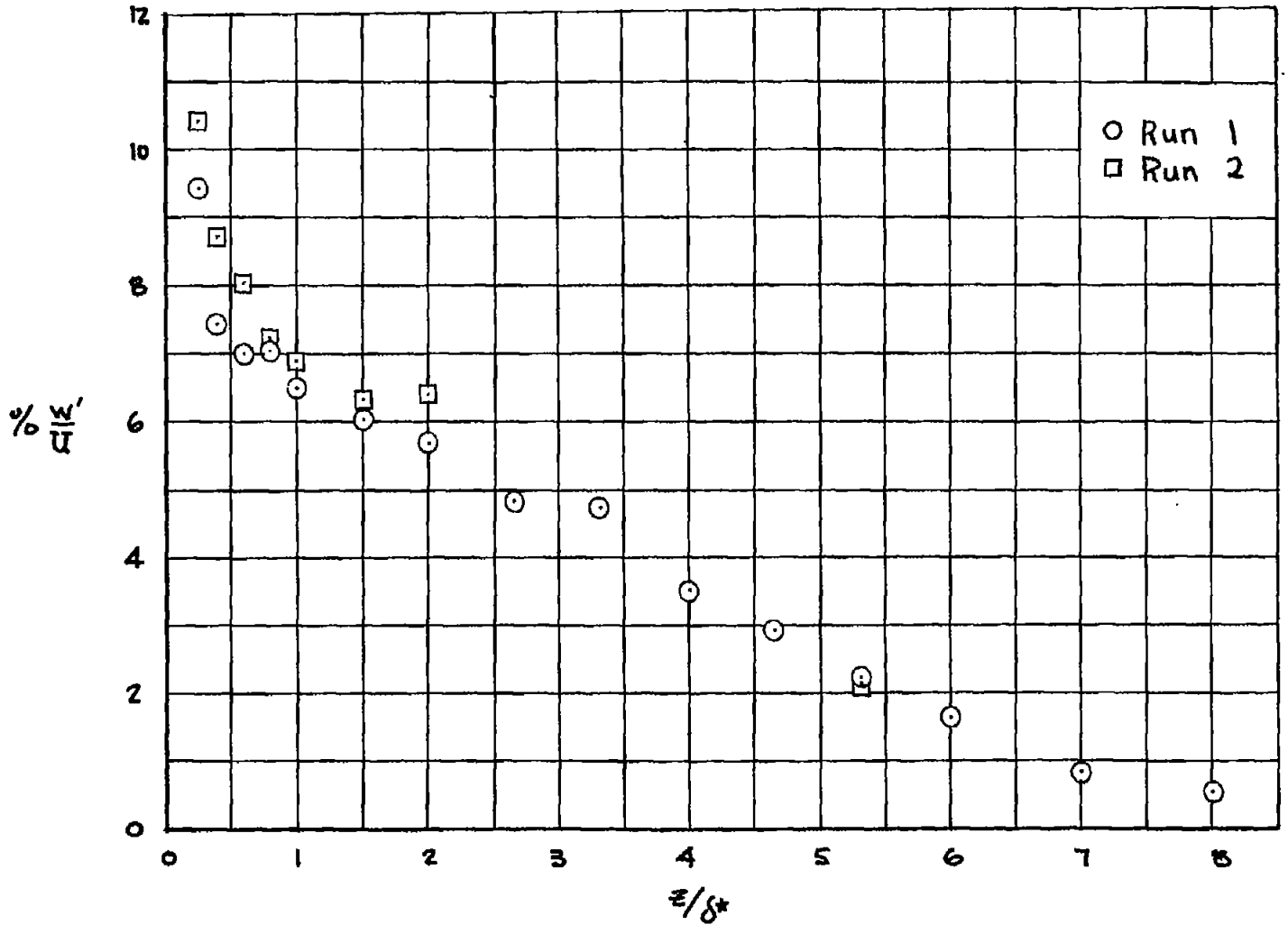

(a) Measurements taken 24 inches from leading edge.

Figure 5.- Lateral turbulence intensity. $\Lambda = 0^{\circ}$.

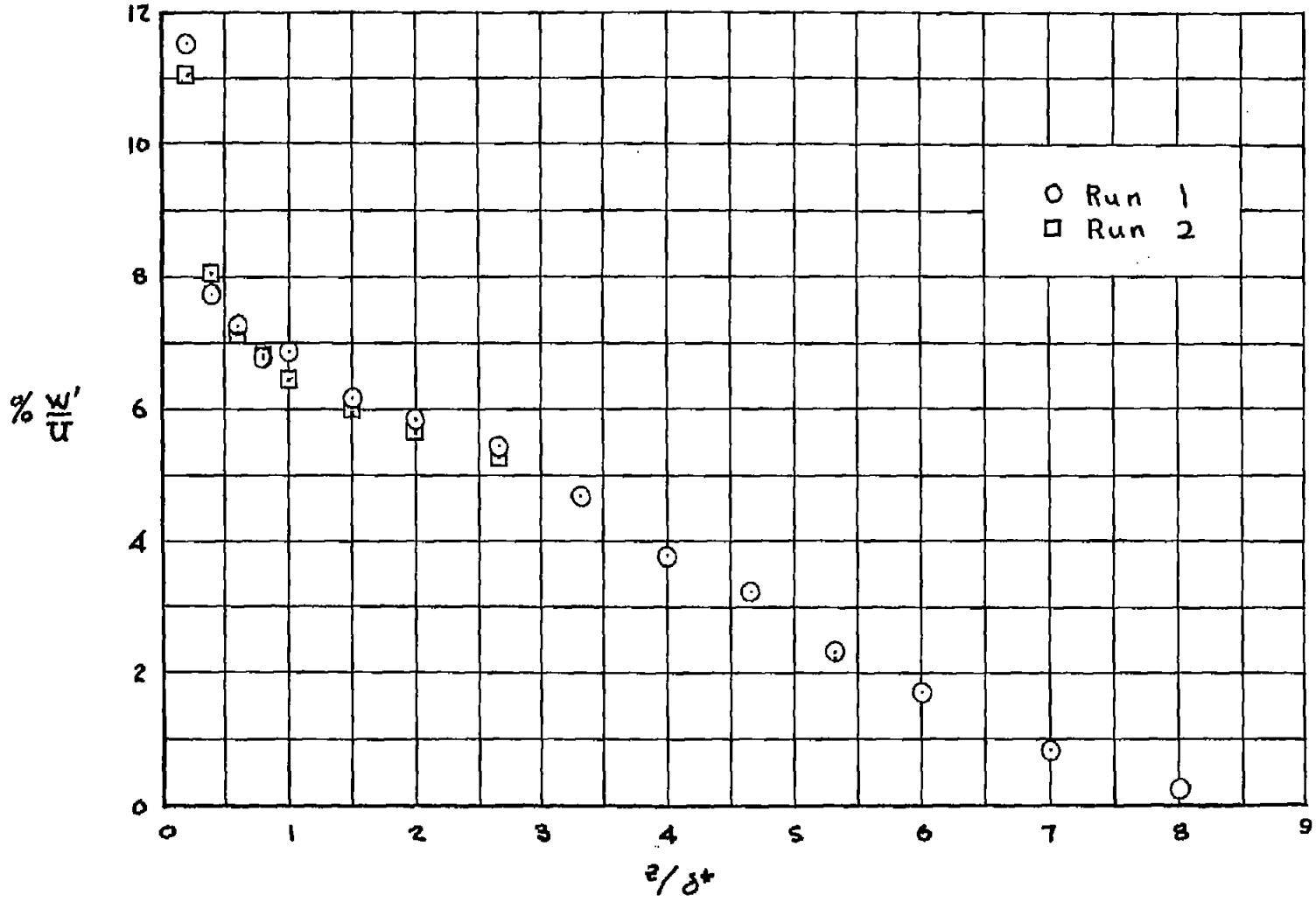

(b) Measurements taken 36 inches from leading edge.

Figure 5.- Continued.

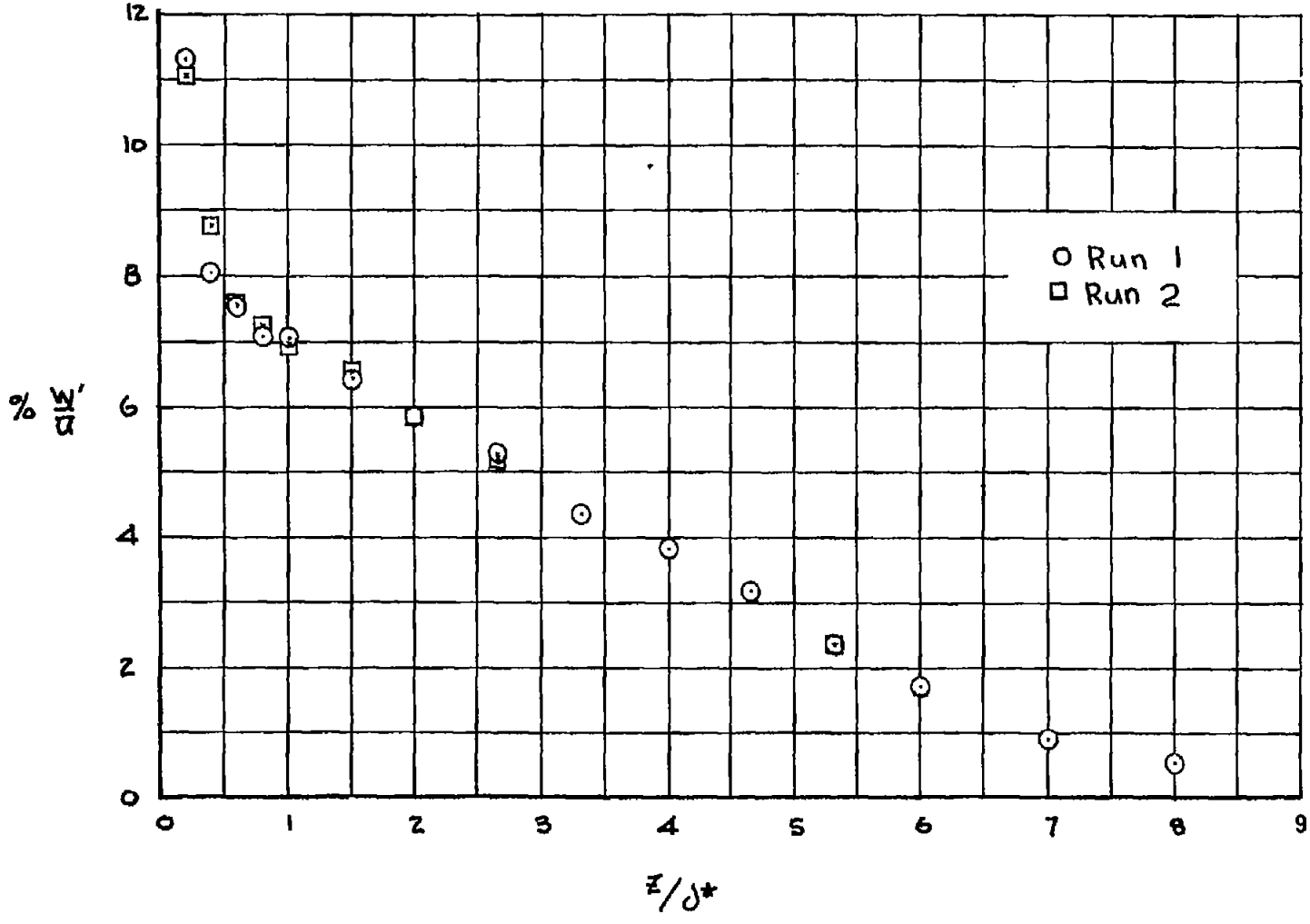

(c) Measurements taken 47 inches from leading edge.

Figure 5.- Concluded.

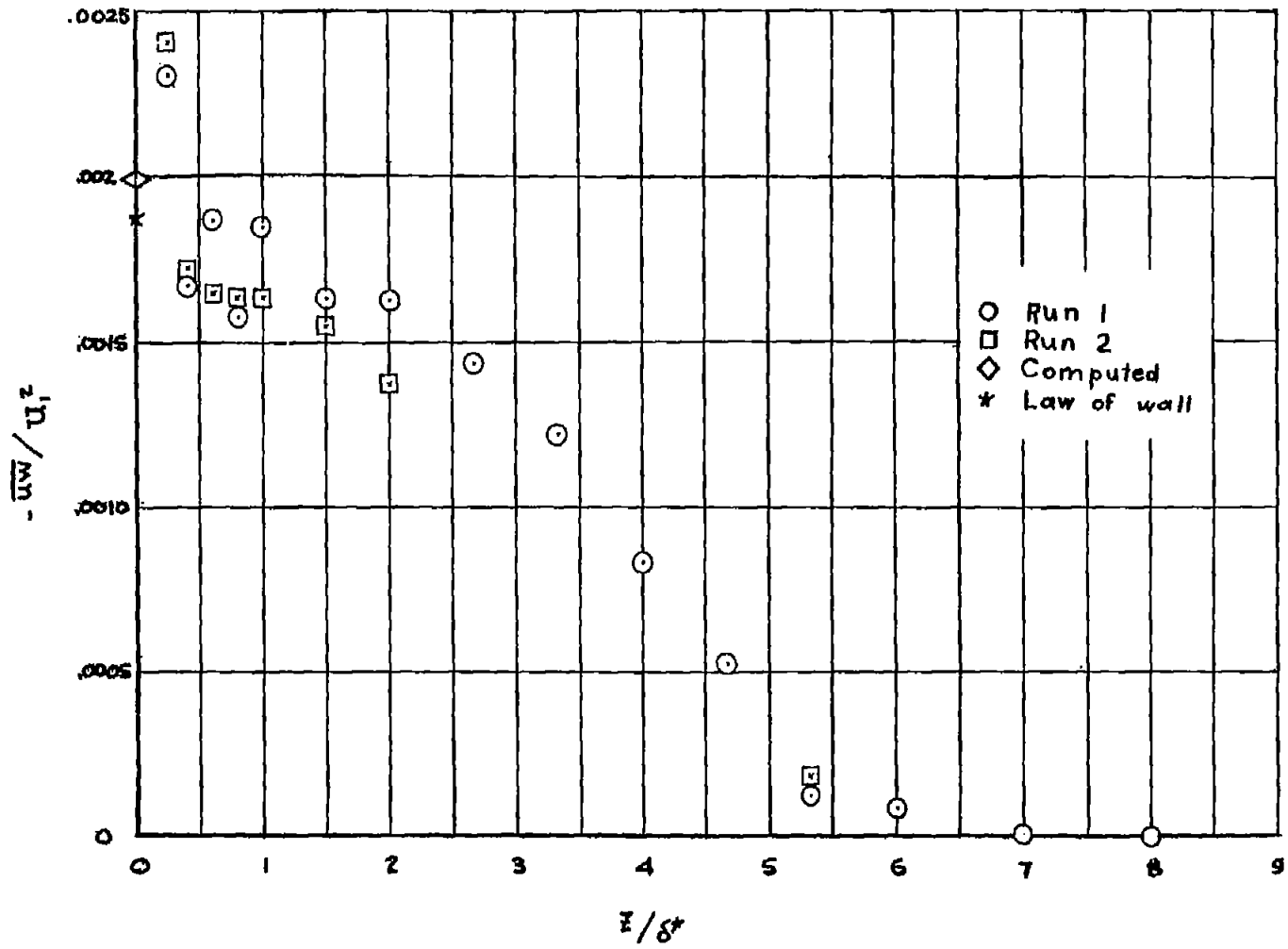

(a) Measurements taken 24 inches from leading edge.

Figure 6.- Turbulent-shearing-stress distribution. $\Lambda = 0^\circ$. Computed data obtained using $\partial\vartheta/\partial(\xi_0 + \xi)$.

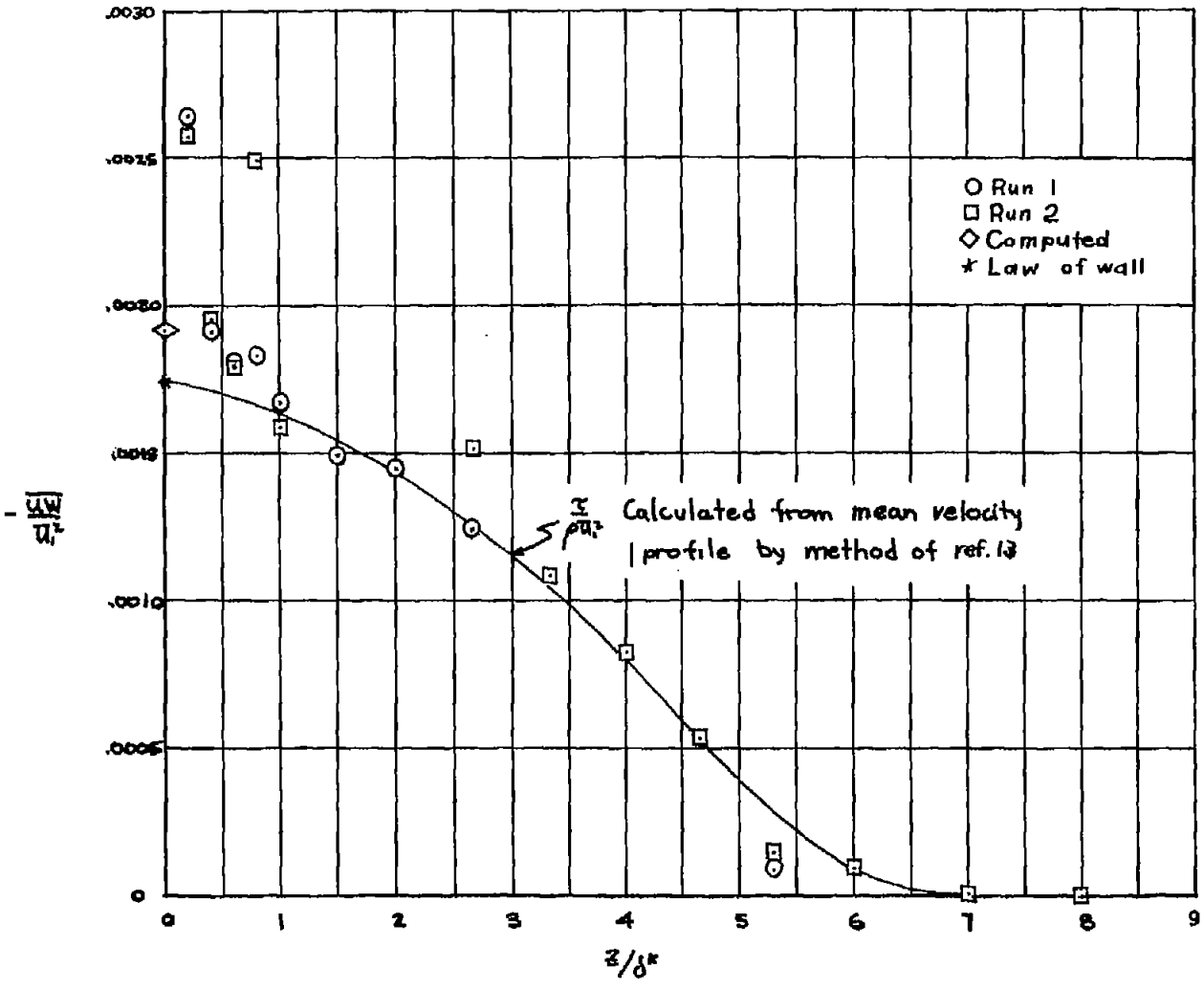

(b) Measurements taken 36 inches from leading edge.

Figure 6.- Continued.

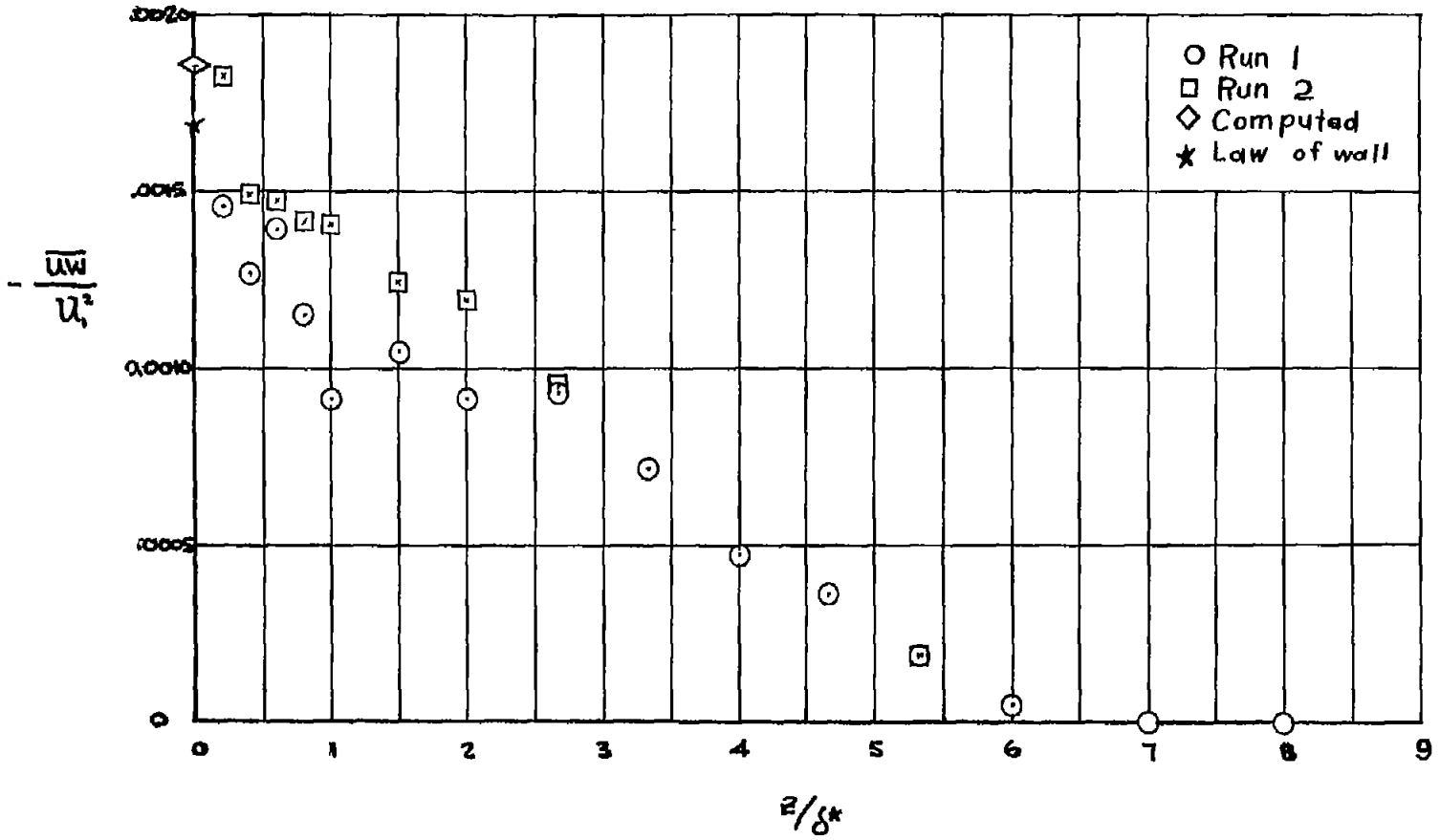

(c) Measurements taken 47 inches from leading edge.

Figure 6.- Concluded.

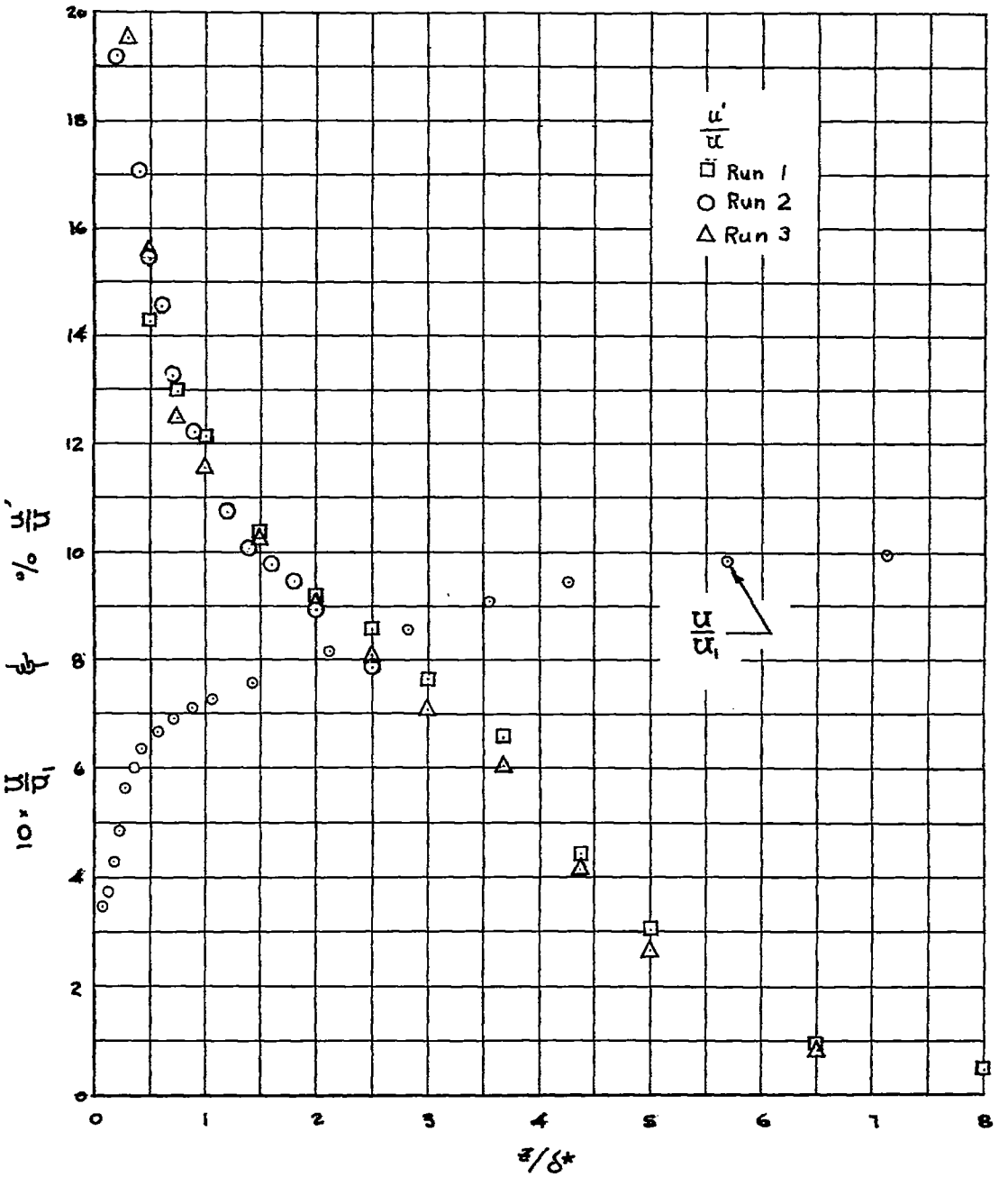

(a) $\delta^* = 0.070$ inch; $\vartheta = 0.049$ inch; measurements taken 8 inches from leading edge.

Figure 7.- Mean velocity and longitudinal turbulence intensity. $\Lambda = 45^\circ$; Re = 250,000 per foot.

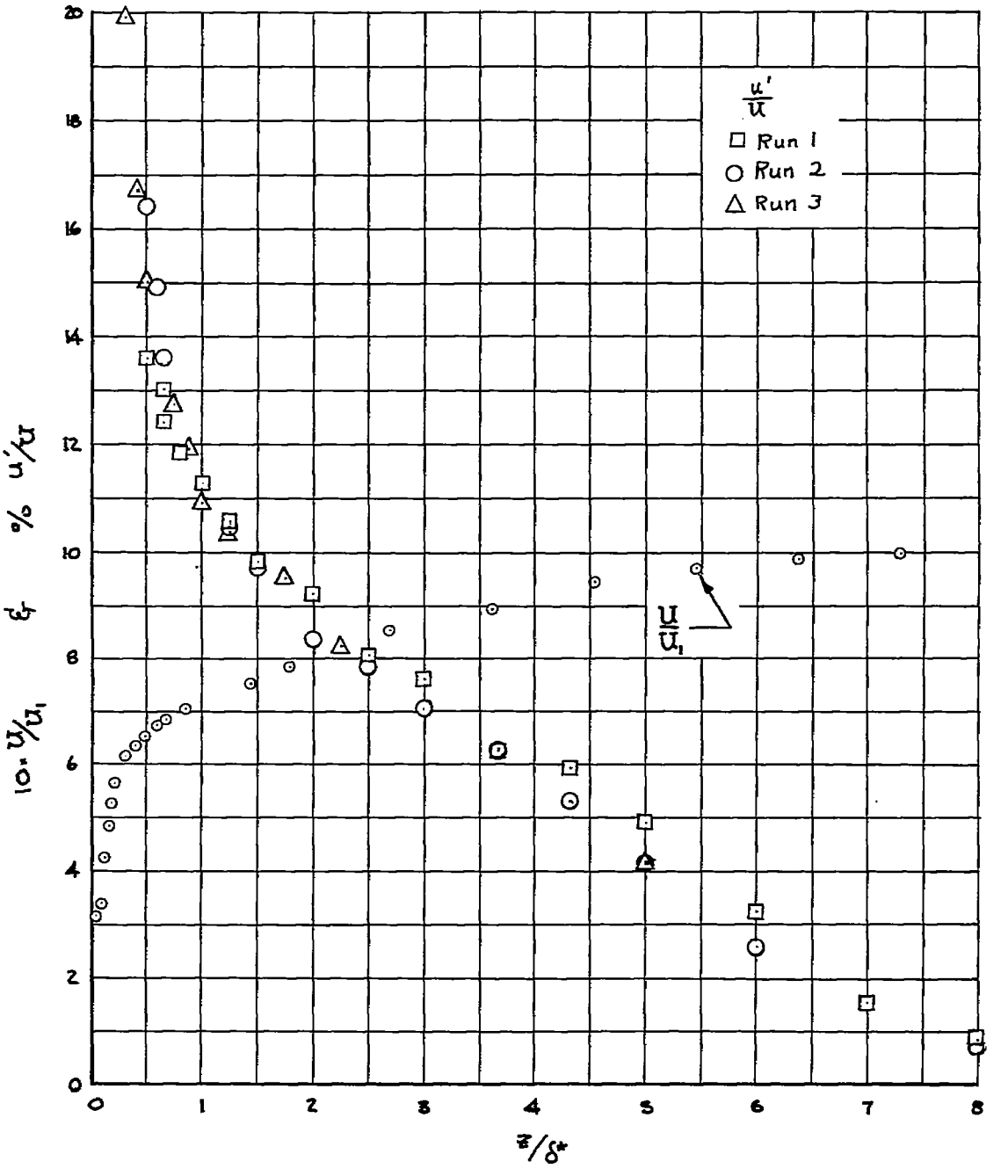

(b) $\delta^* = 0.109$ inch; $\vartheta = 0.080$ inch; measurements taken 24 inches from leading edge.

Figure 7.- Continued.

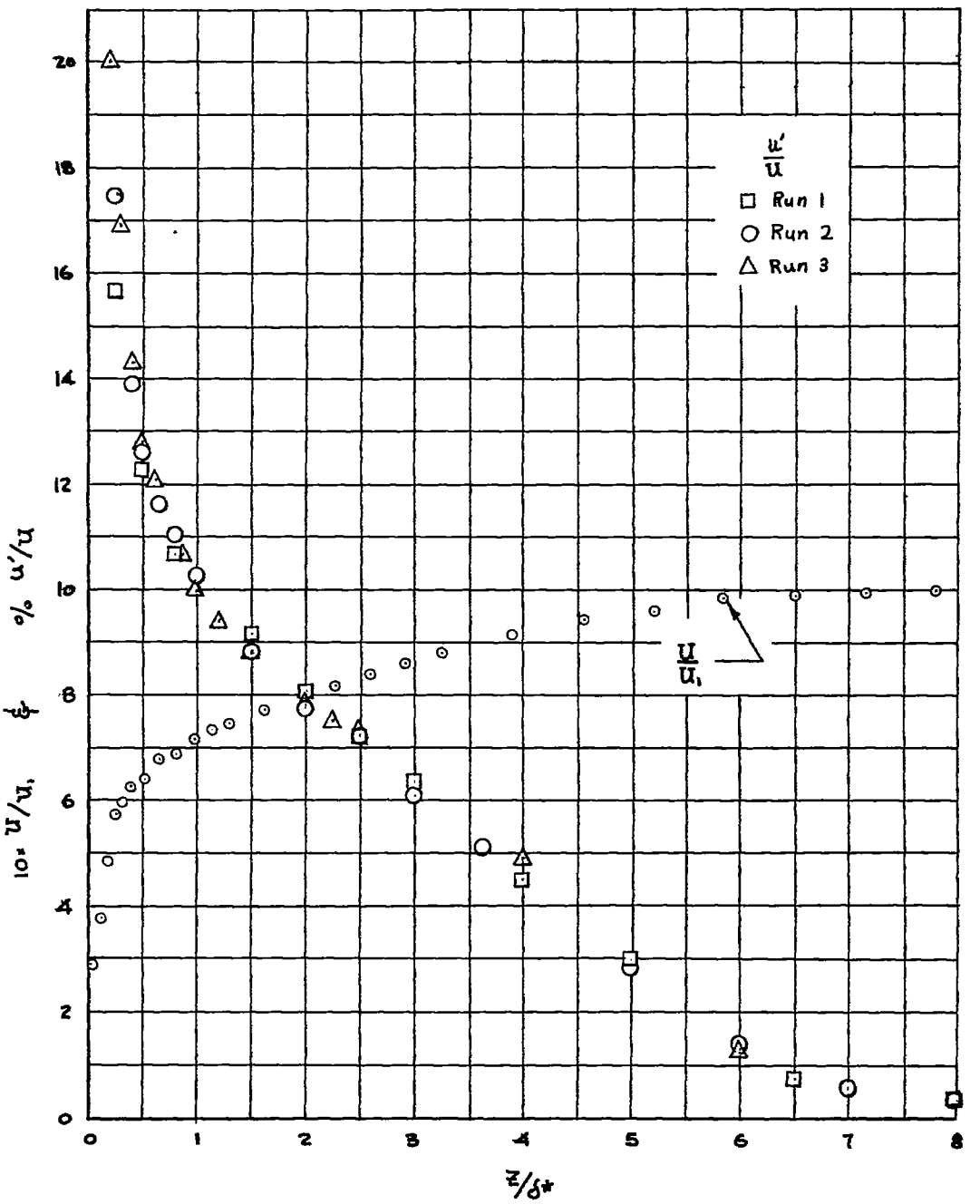

(c) $\delta^* = 0.154$ inch; $\vartheta = 0.111$ inch; measured 36 inches from leading edge.

Figure 7.- Continued.

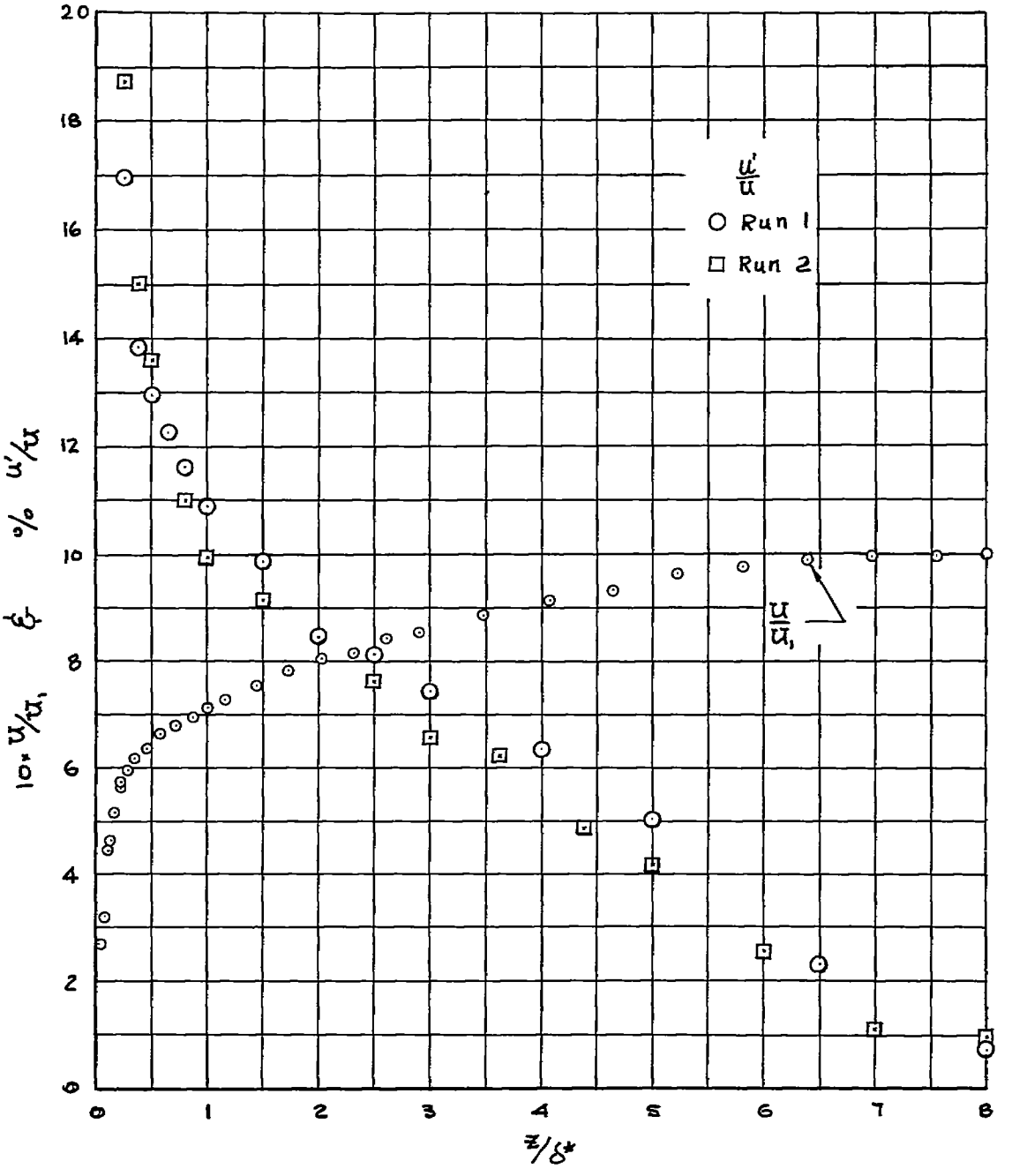

(d) $\delta^* = 0.1725$ inch; $\vartheta = 0.127$ inch; measurements taken 44 inches from leading edge.

Figure 7.- Continued.

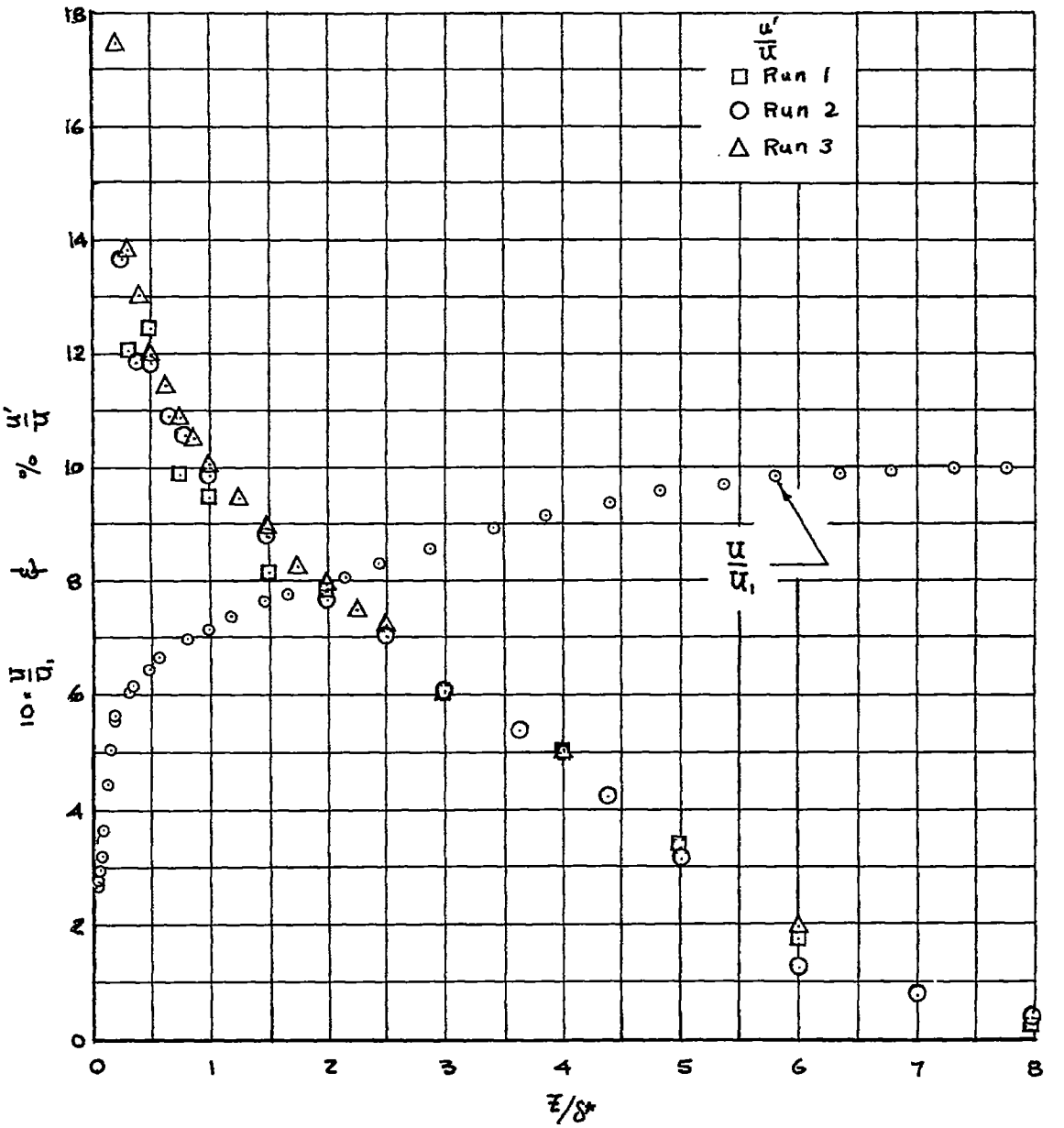

(e) $\delta^* = 0.205$ inch; $\vartheta = 0.145$ inch; measurements taken 54 inches from leading edge.

Figure 7.- Continued.

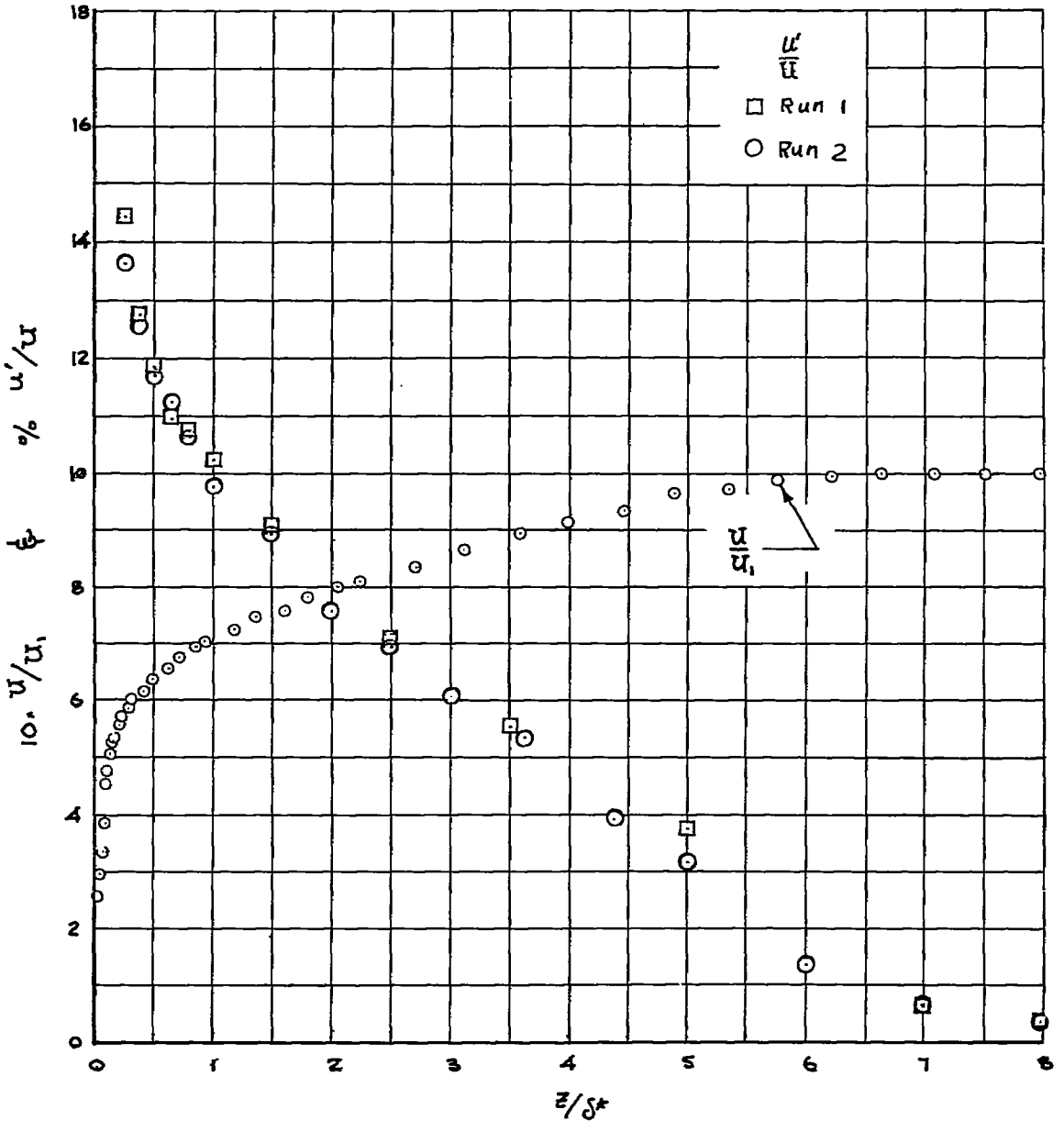

(f) $\delta^* = 0.228$ inch; $\vartheta = 0.165$ inch; measurements taken 66 inches from leading edge.

Figure 7.- Concluded.

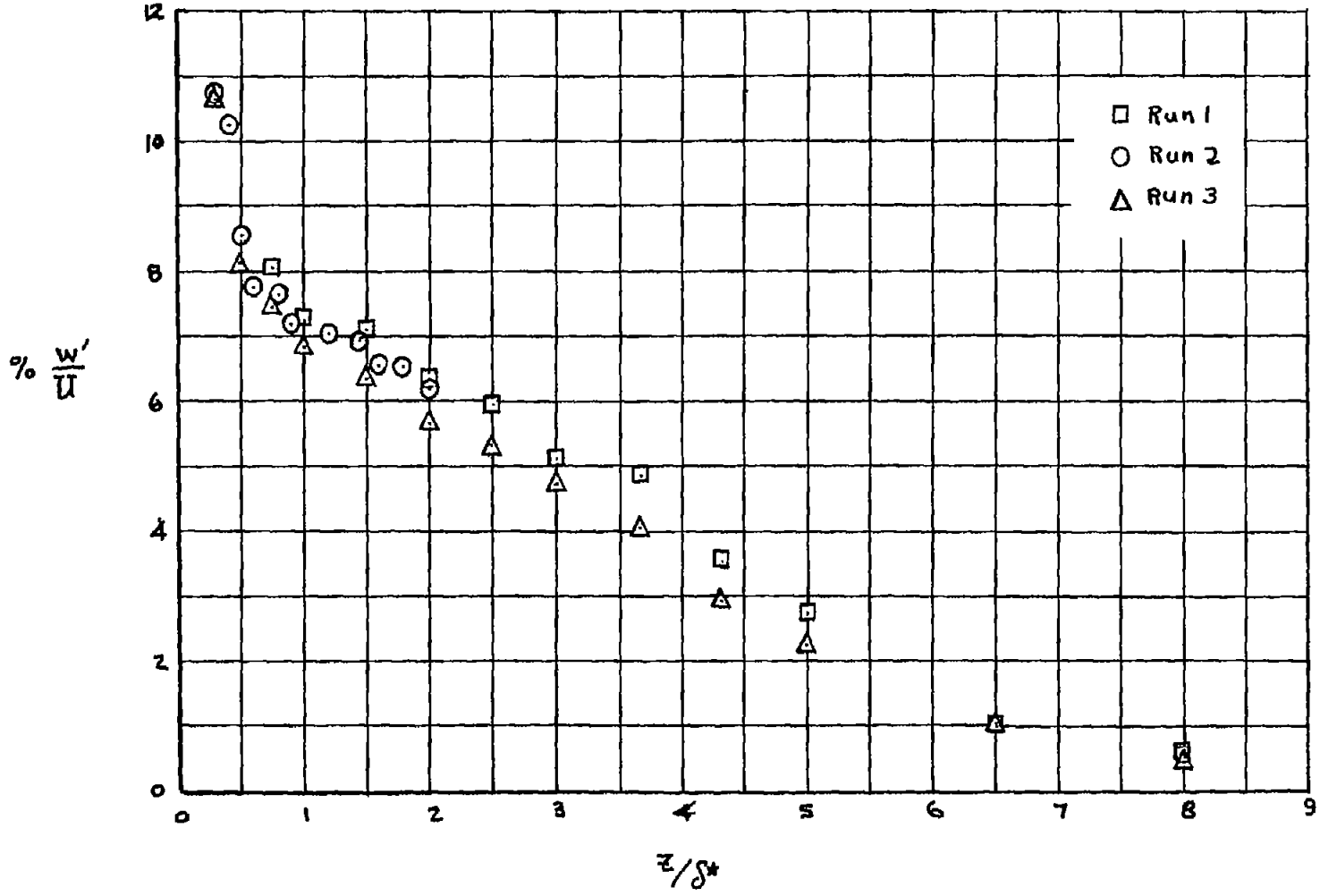

(a) Measurements taken 8 inches from leading edge.

Figure 8.- Lateral turbulence intensity. $\Lambda = 45^{\circ}$.

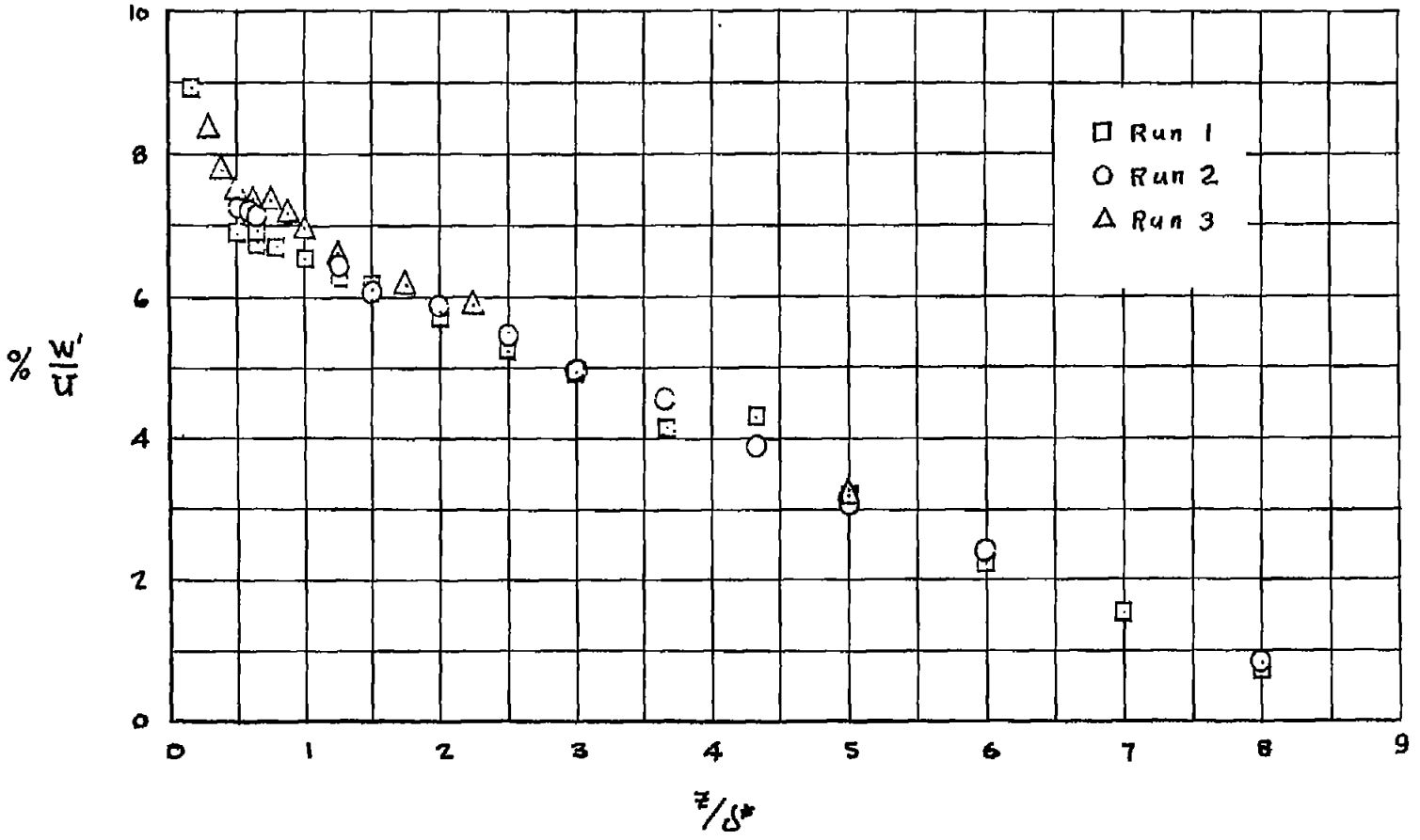

(b) Measurements taken 24 inches from leading edge.

Figure 8.- Continued.

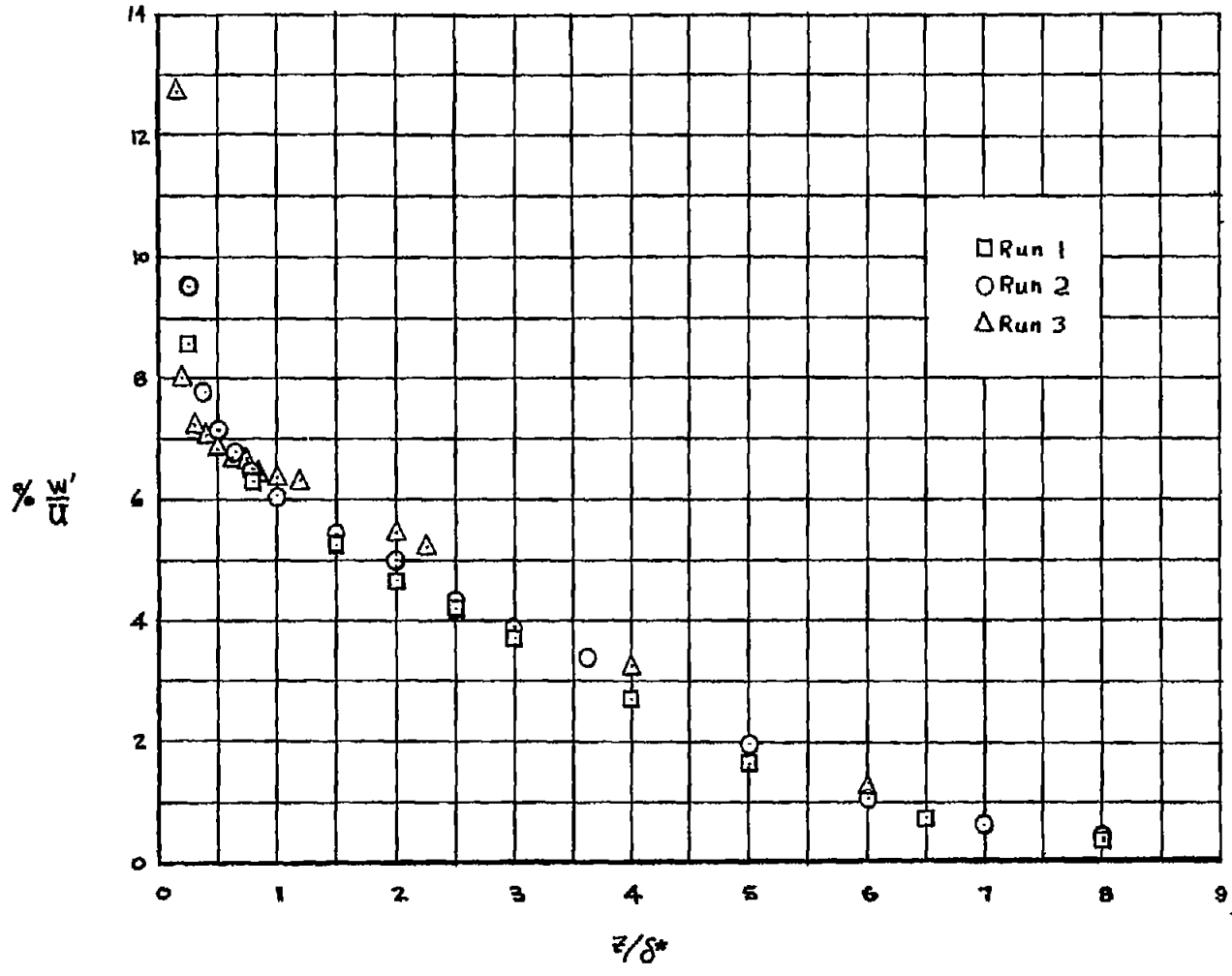

(c) Measurements taken 36 inches from leading edge.

Figure 8.- Continued.

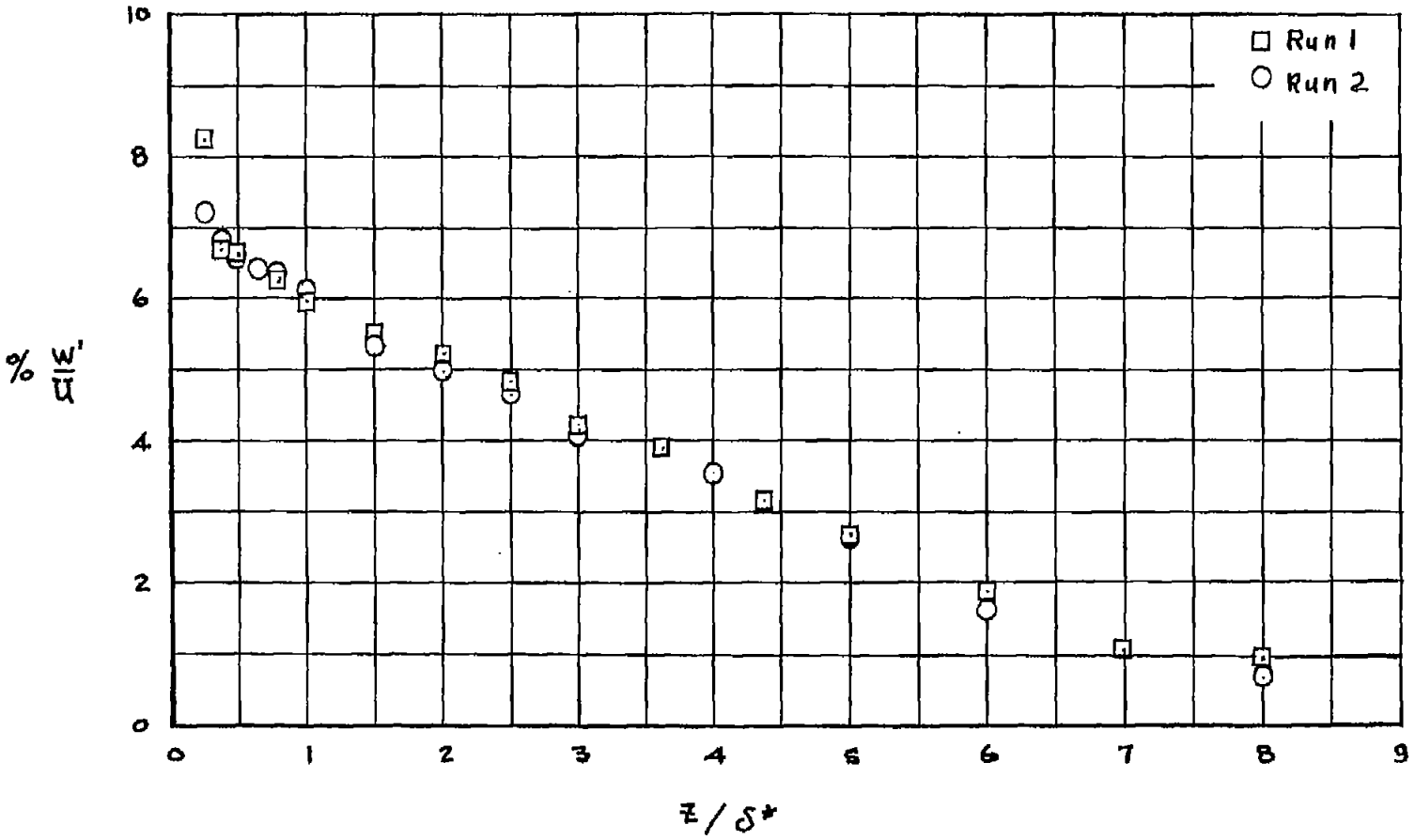

(d) Measurements taken 44 inches from leading edge.

Figure 8.- Continued.

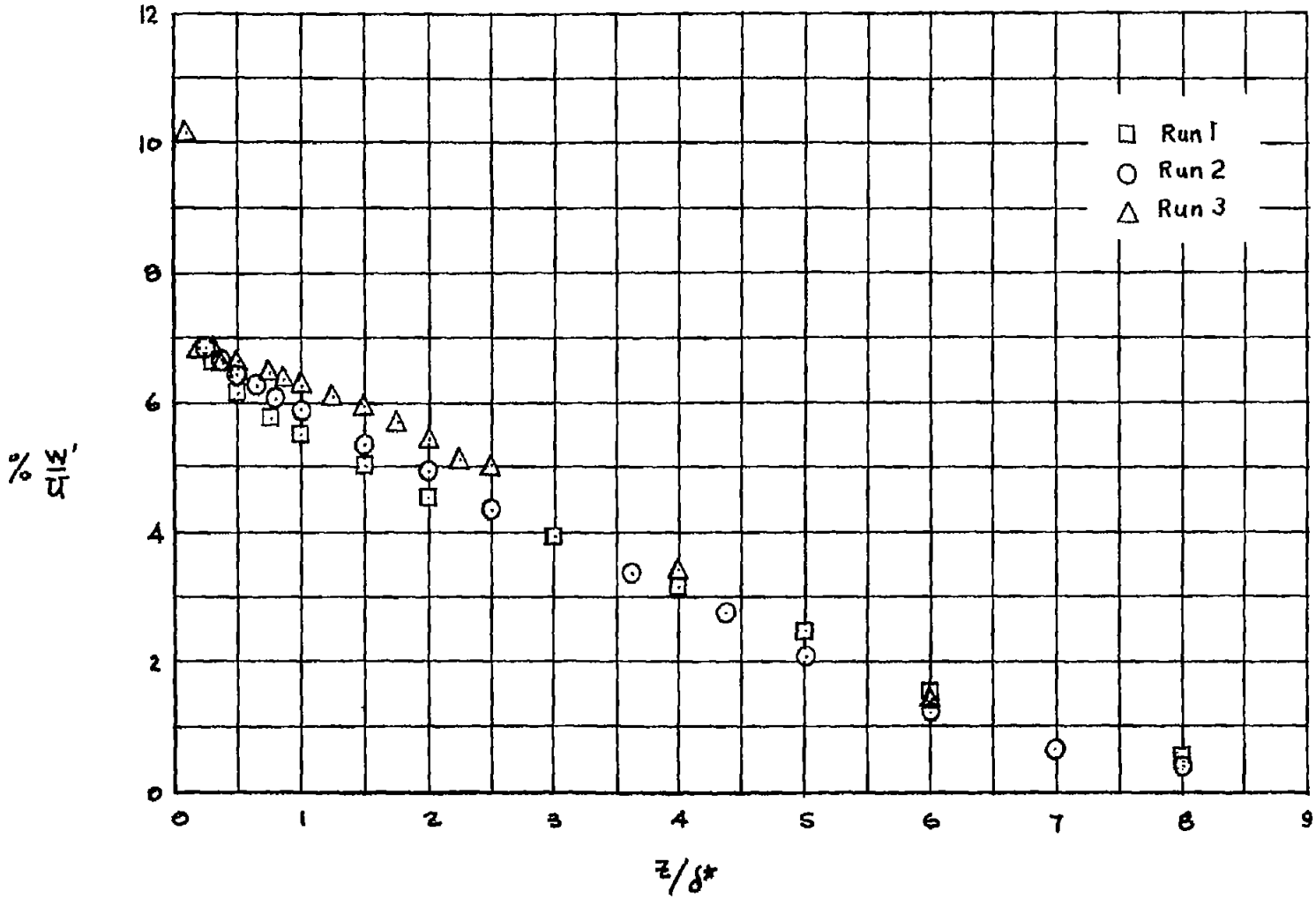

(e) Measurements taken 54 inches from leading edge.

Figure 8.- Continued.

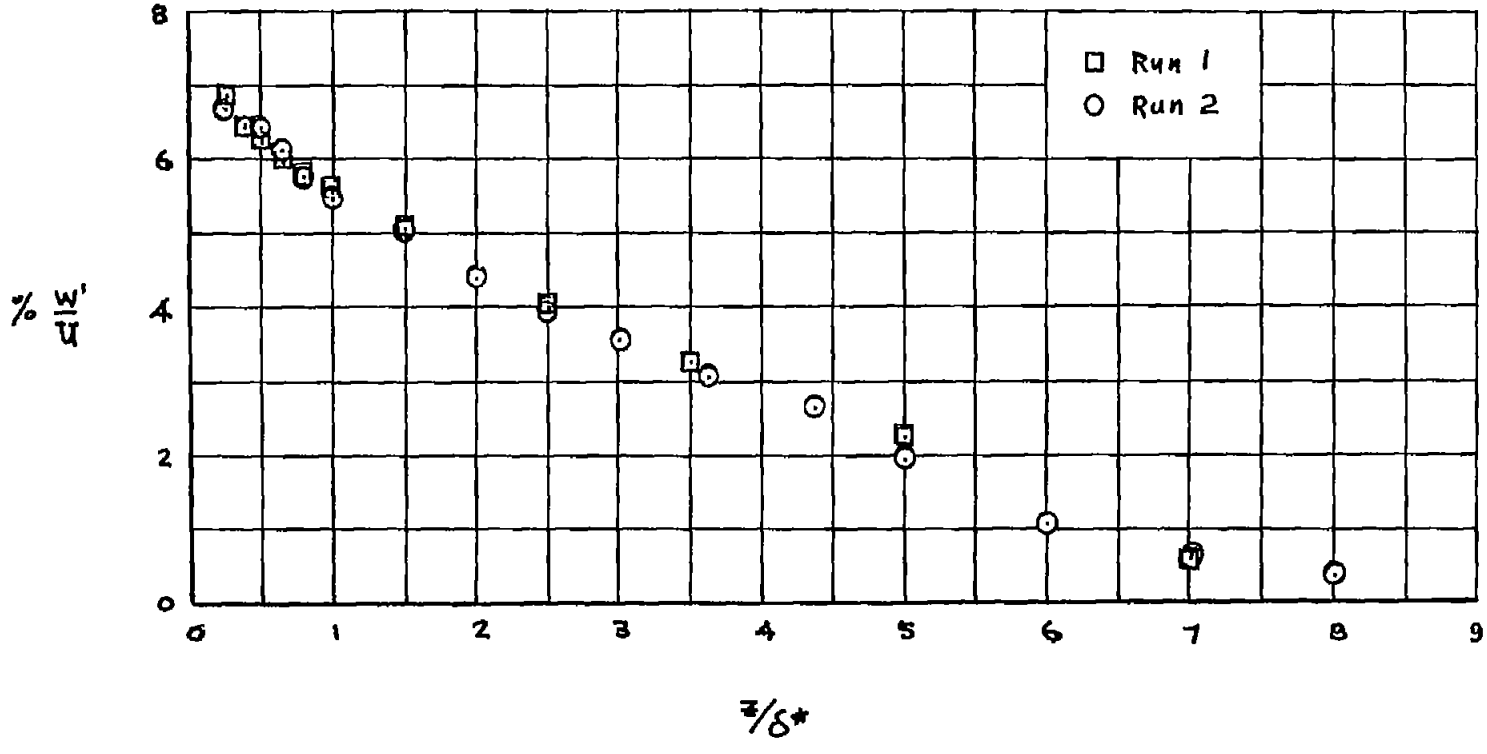

(f) Measurements taken 66 inches from leading edge.

Figure 8.- Concluded.

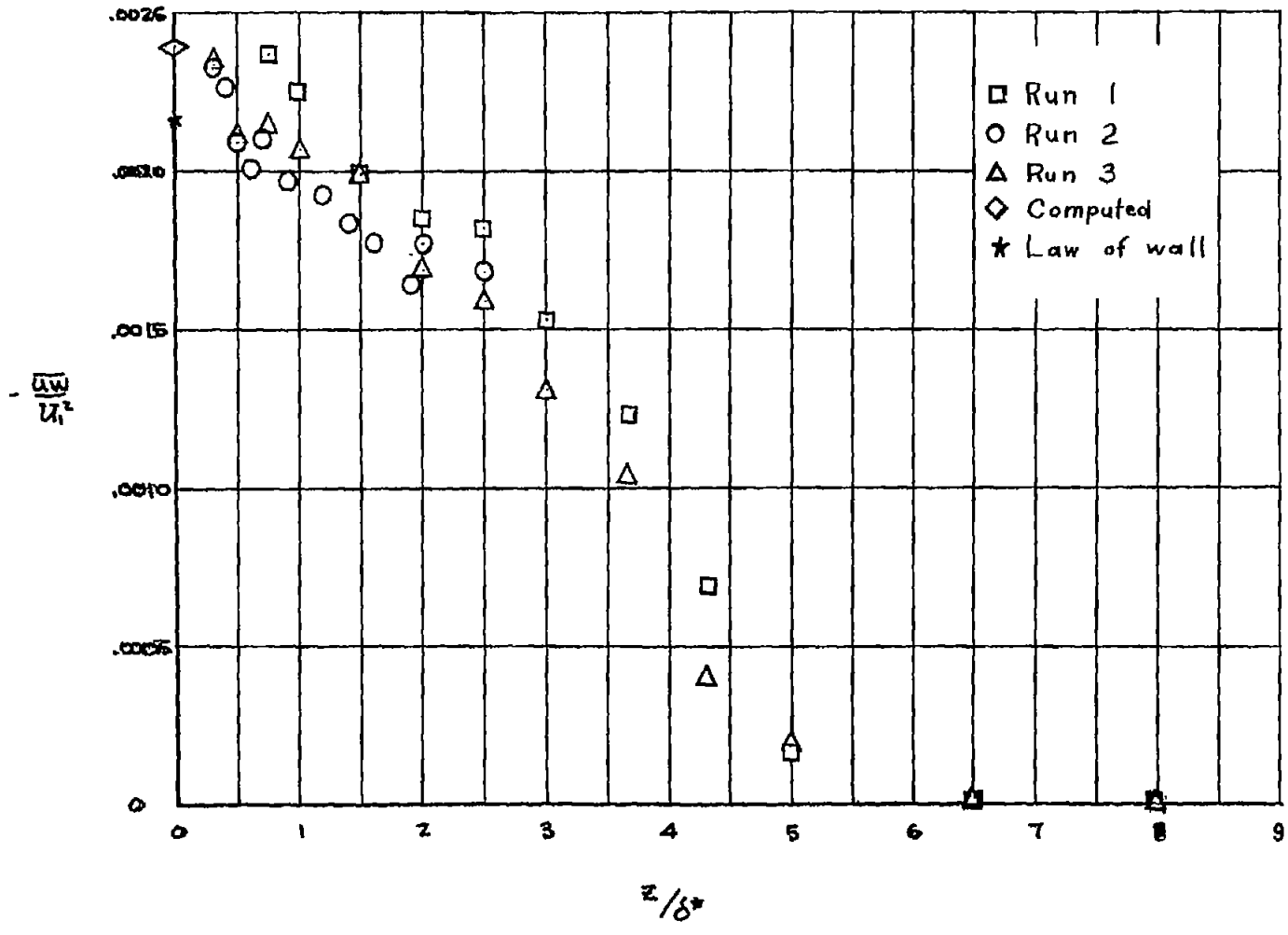

(a) Measurements taken 8 inches from leading edge.

Figure 9.- Turbulent-shearing-stress distribution. $\Lambda = 45^\circ$. Computed data obtained using $\partial\vartheta/\partial(\xi_0 + \xi)$.

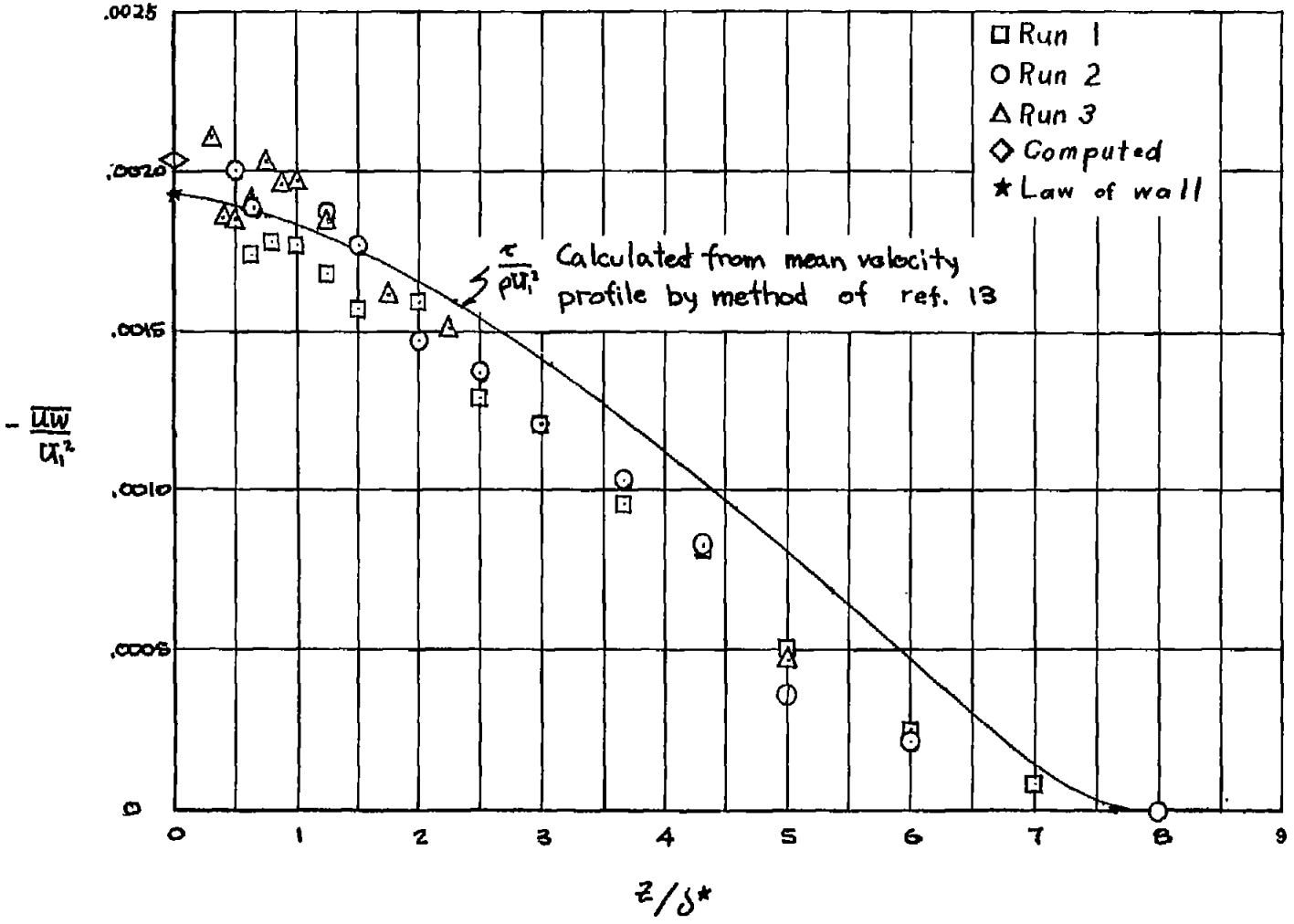

(b) Measurements taken 24 inches from leading edge.

Figure 9.- Continued.

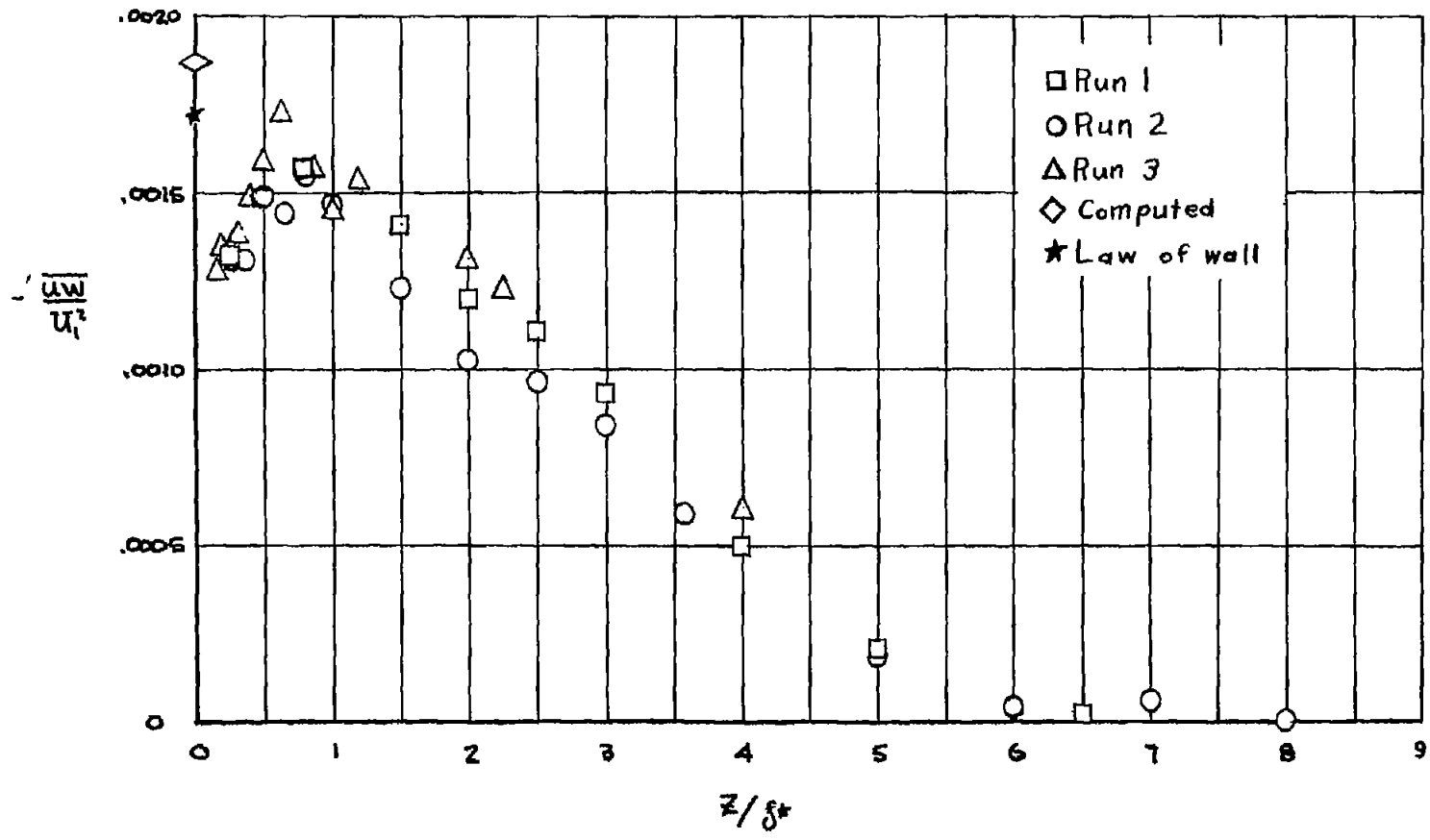

(c) Measurements taken 36 inches from leading edge.

Figure 9.- Continued.

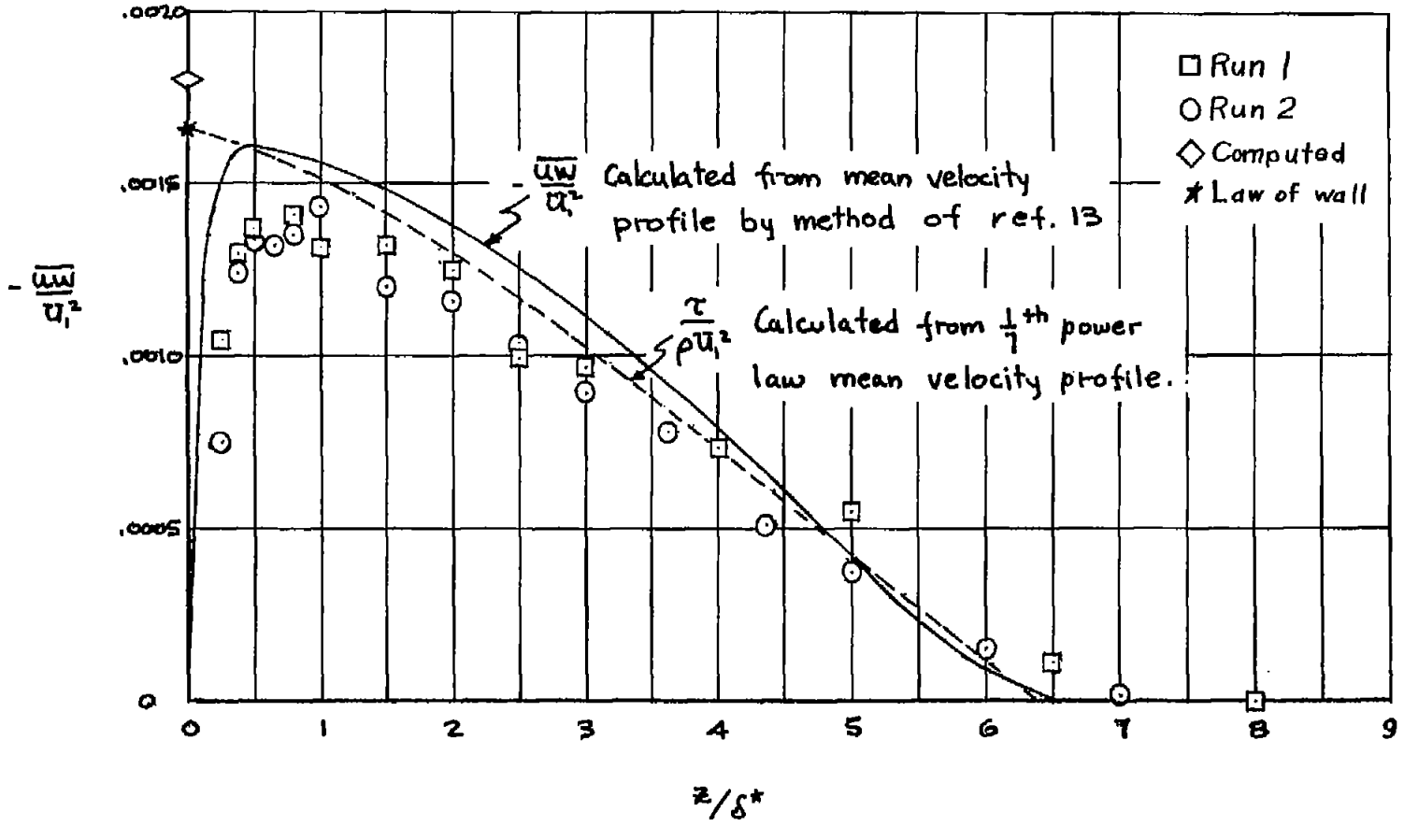

(d) Measurements taken 44 inches from leading edge.

Figure 9.- Continued.

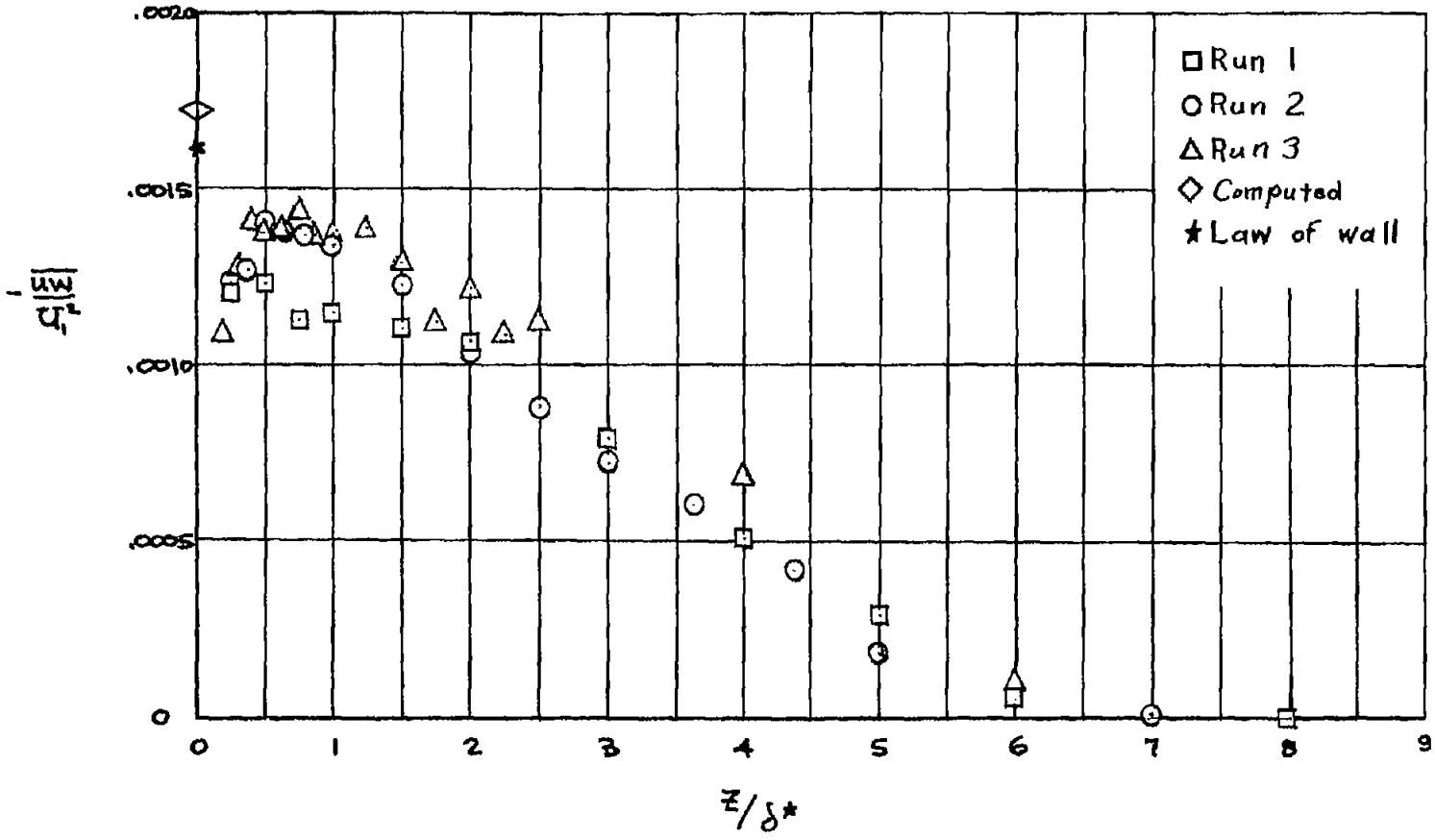

(e) Measurements taken 54 inches from leading edge.

Figure 9.- Continued.

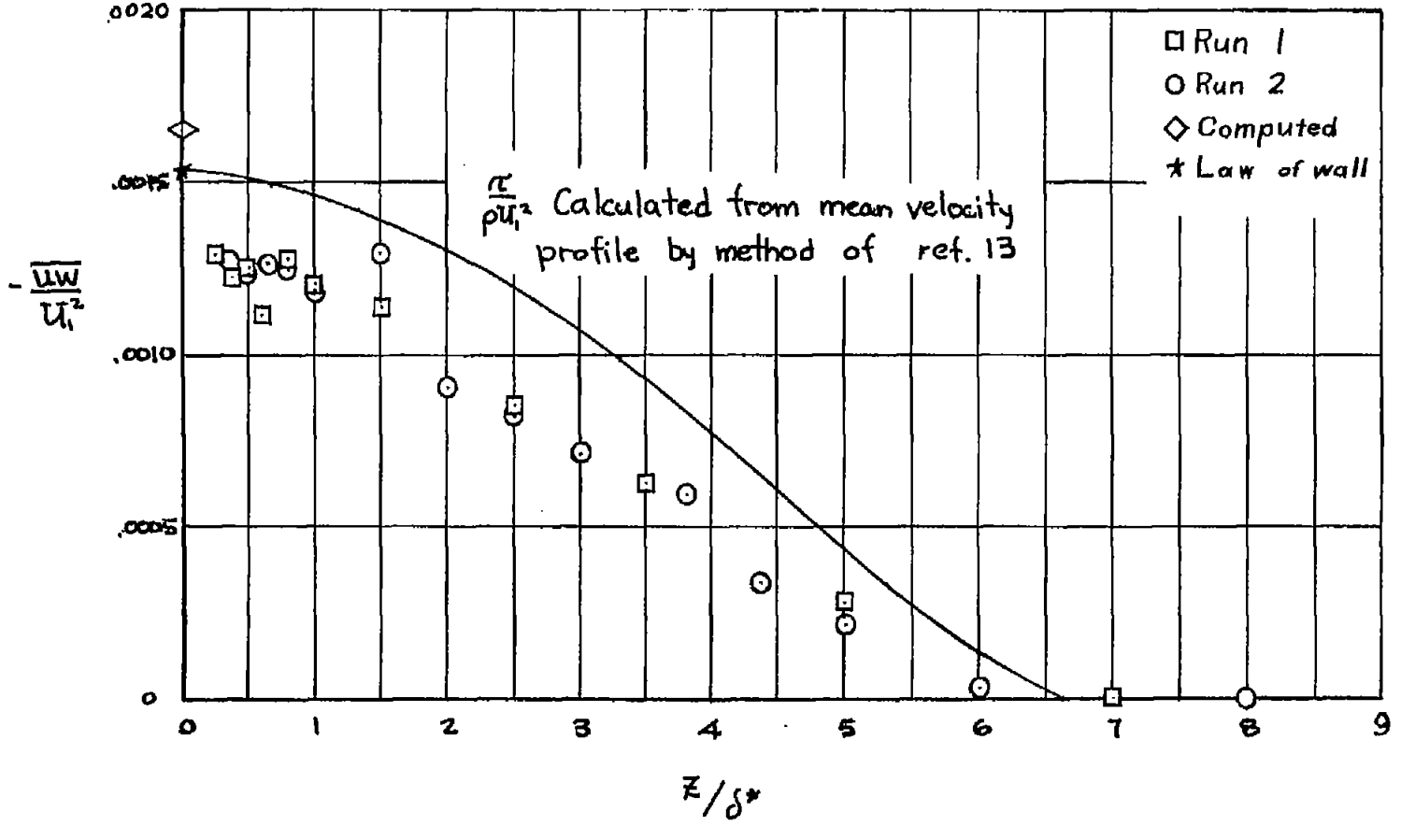

(f) Measurements taken 66 inches from leading edge.

Figure 9.- Concluded.

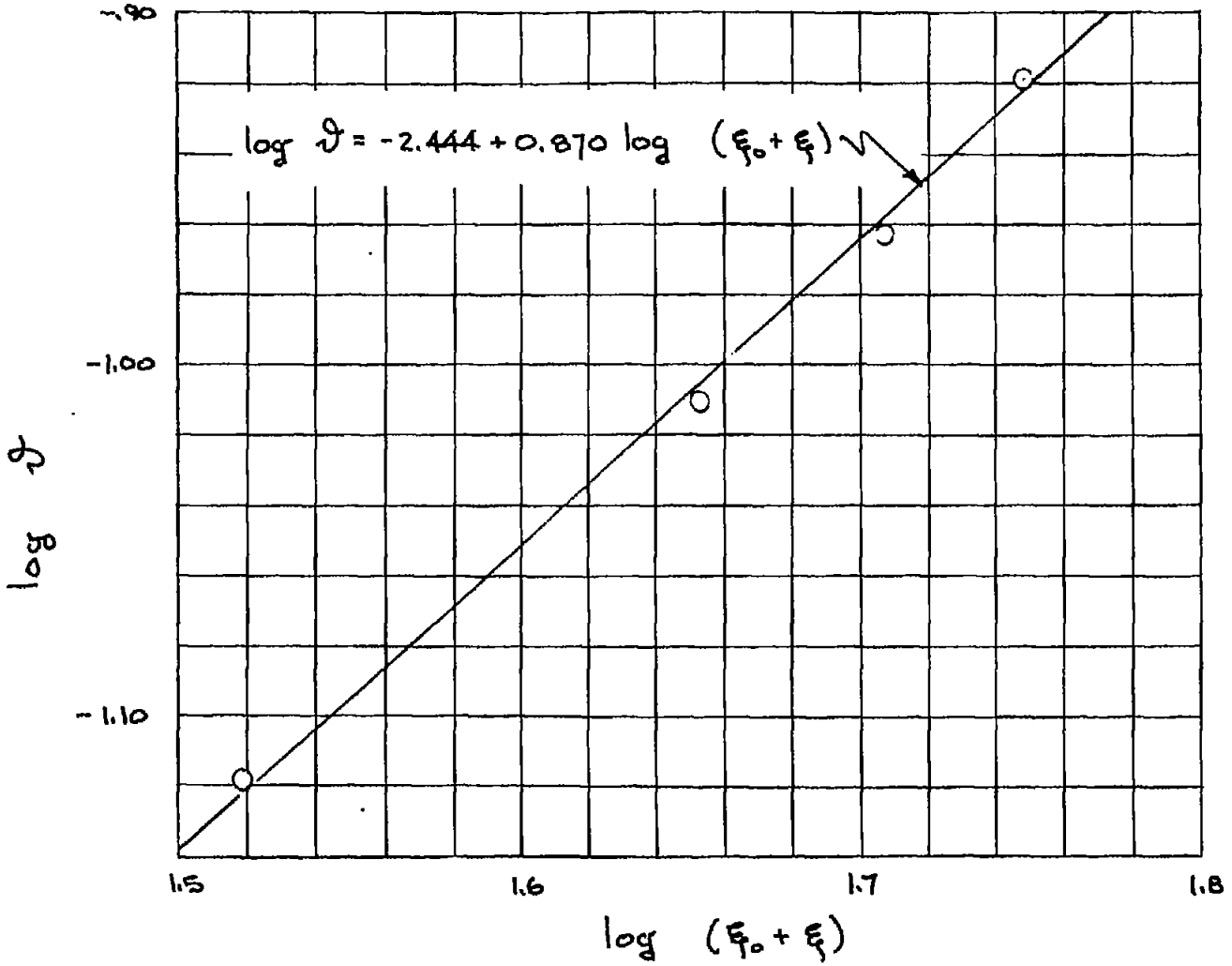

Figure 10.- Momentum thickness growth. $\Lambda = 0^{\circ}$; Re = 250,000 per foot.

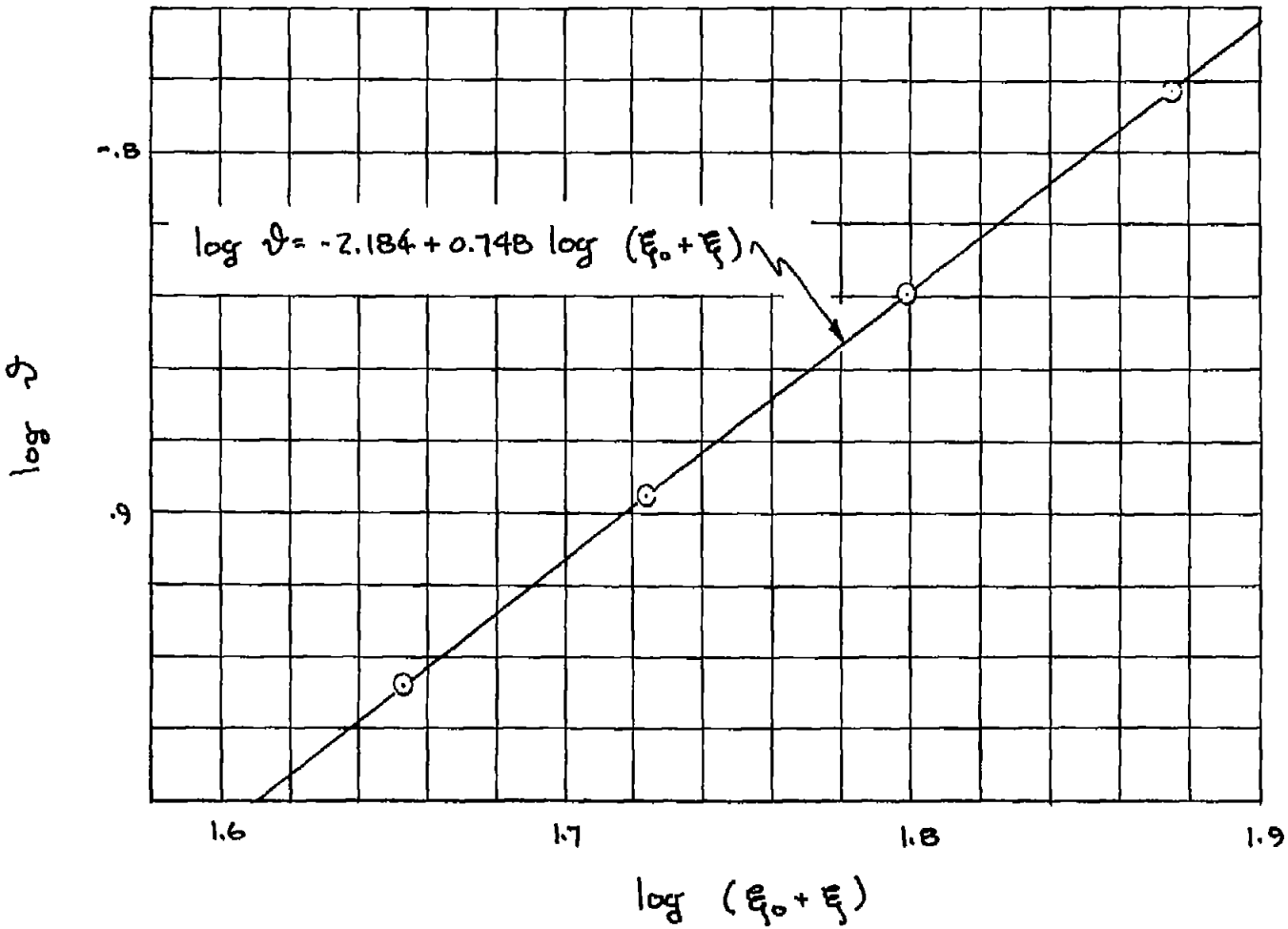

Figure 11.- Momentum thickness growth. $\Lambda = 45^{\circ}$; Re = 250,000 per foot.

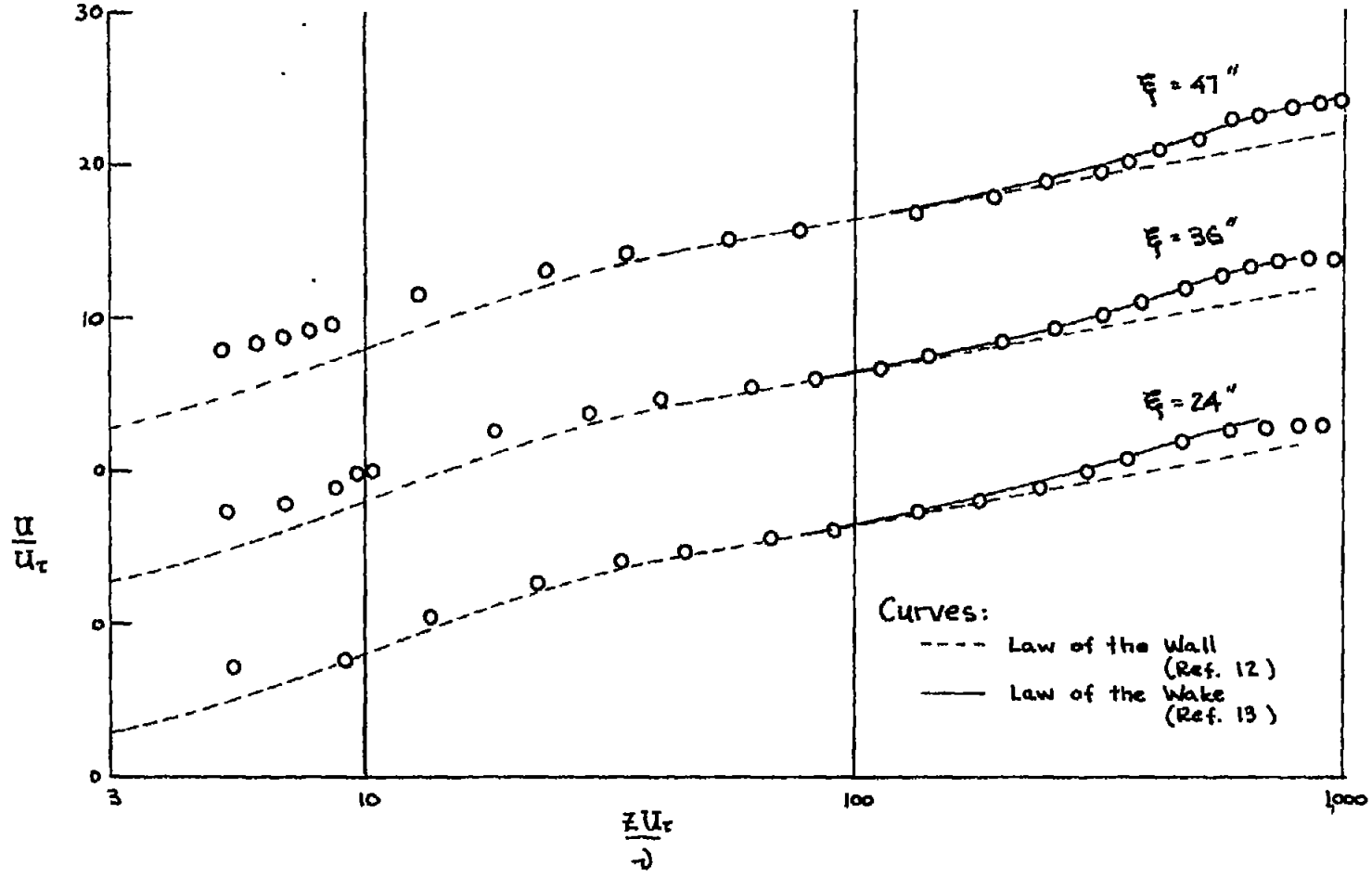

(a) $\Lambda = 0^\circ$.

Figure 12.- Mean velocity profiles. Re = 250,000 per foot.

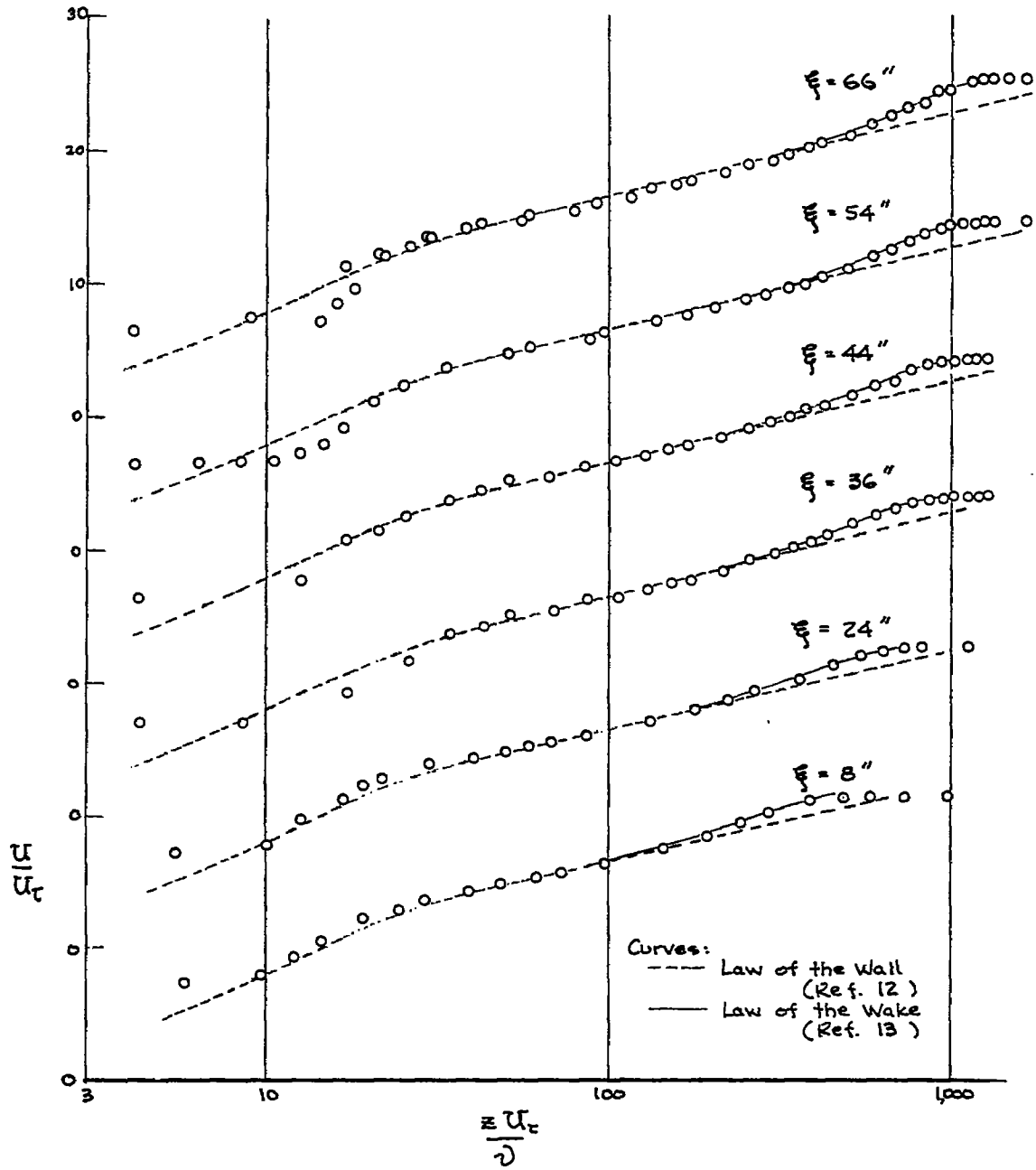

(b) $\Lambda = 45^{\circ}$.

Figure 12.- Concluded.

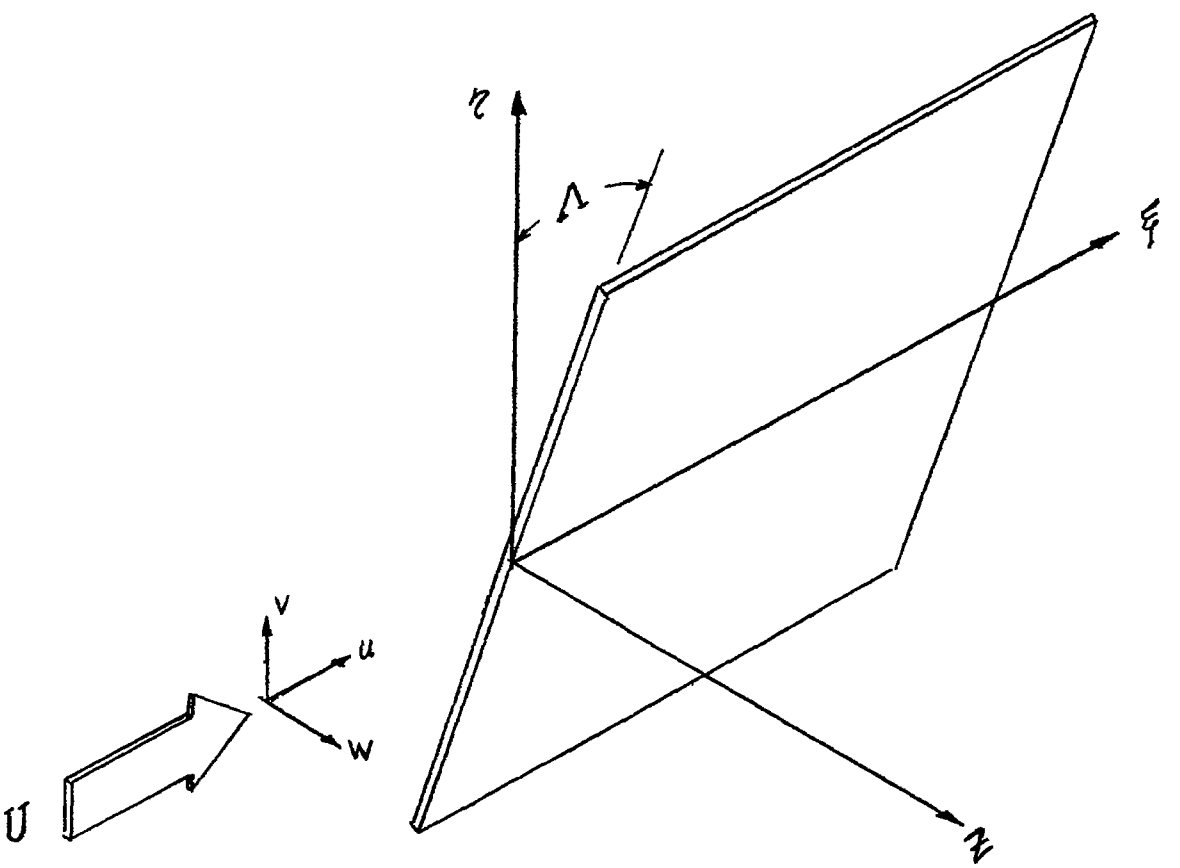

Figure 13.- Coordinate system for yawed flat plate.

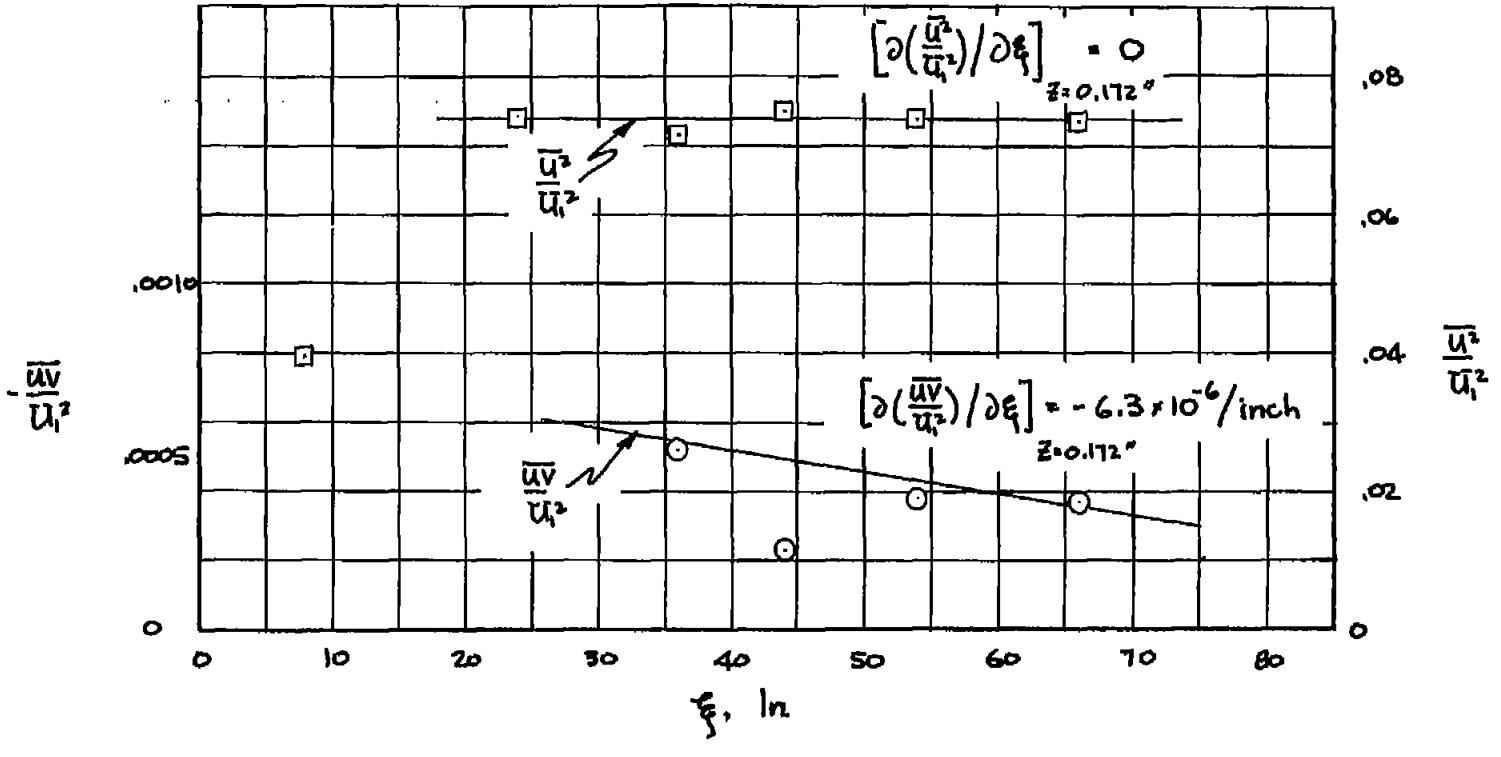

Figure 14.- Estimation of additional terms in Turcotte's (ref. 6) equation of motion.

$$U\frac{\partial U}{\partial \xi} + W\frac{\partial U}{\partial z} = \frac{1}{\rho}\left(\mu\frac{\partial^2 U}{\partial z^2} - \rho\frac{\partial \overline{uw}}{\partial z} - \rho\frac{\partial \overline{u^2}}{\partial \xi} + \rho\frac{\partial \overline{uv}}{\partial \xi}\right); \quad \left[\partial\left(\frac{\overline{uw}}{U_1^2}\right)\Big/\partial z\right] = -7.75 \times 10^{-4} \text{ per inch};$$

ξ = 44 inches; z = 0.172 inch.

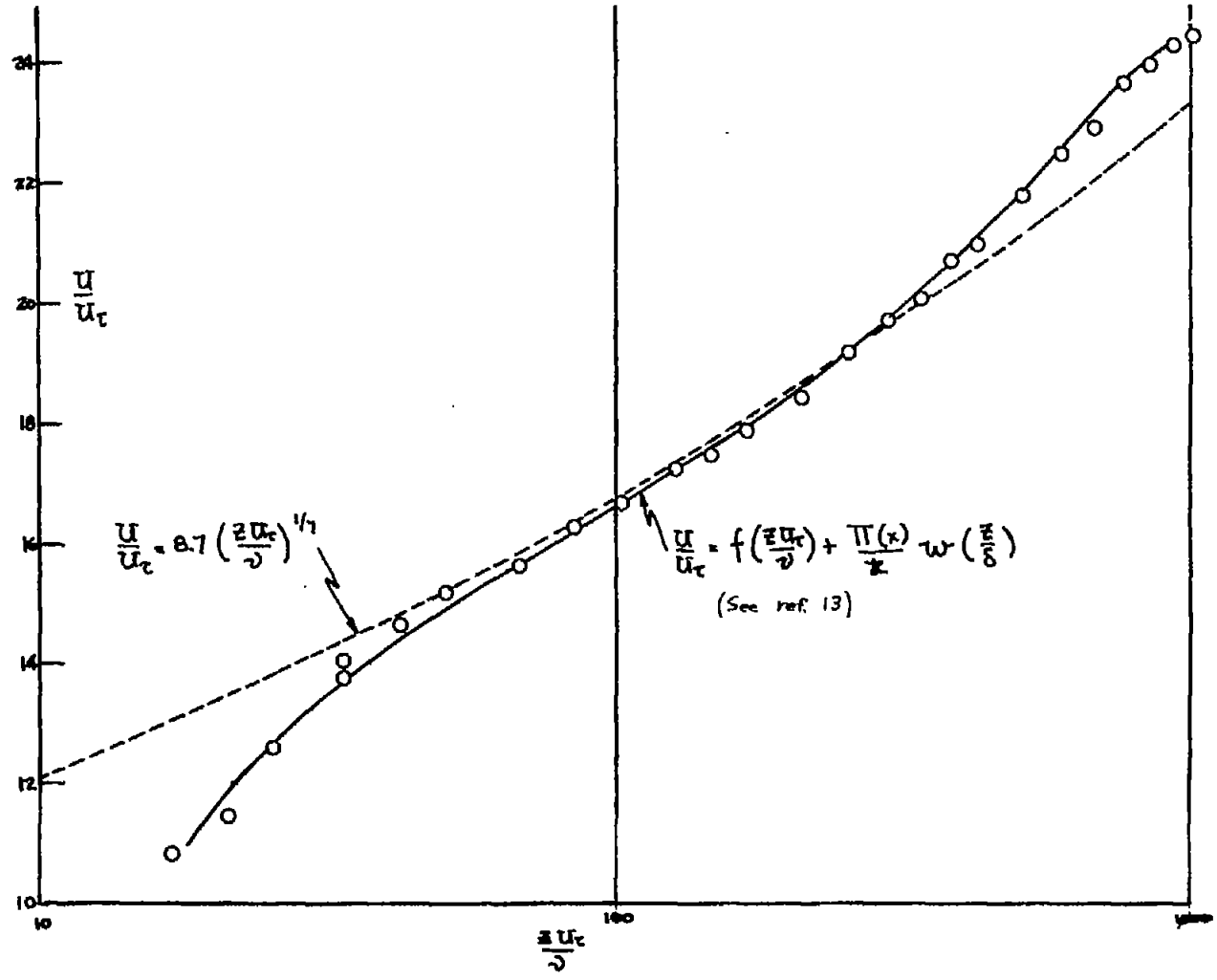

Figure 15.- Mean velocity profile. ξ = 44 inches; Λ = 45°; Re = 250,000 per foot; $\frac{U_1}{U_\tau}$ = 24.56; π = 0.438.